Available online at www.sciencedirect.com
SCIENCE DIRECT®
Coordination Chemistry Reviews 249 (2005) 343–373
COORDINATION CHEMISTRY REVIEWS
www.elsevier.com/locate/ccr

Review

Electron-transfer spectroscopy: donor–acceptor electronic coupling, reorganizational energies, reaction pathways and dynamics

John F. Endicott*, Yuan-Jang Chen, Puhui Xie

Department of Chemistry, Wayne State University, Detroit, Michigan 48202-3929, USA

Received 5 February 2004; accepted 13 August 2004

Contents

* Corresponding author. Tel.: +1 313 577 2607; fax: +1 313 577 8822.
E-mail address: jfe@chem.wayne.edu (J.F. Endicott).

doi:10.1016/j.ccr.2004.08.013

Abstract

The emission spectra of several classes of transition metal complexes are examined for relationships between strong donor/acceptor (D/A) electronic coupling (expressed by the matrix element, H_{RP}) and the Franck-Condon (FC) parameters in electron-transfer systems. The effects of large values of H_{RP} on the FC parameters are expressed in terms of the configurational mixing of the diabatic electron-transfer states are interpreted in terms of the fraction of electron density that is delocalized (α^2_{RP}), and they are evaluated with respect to the limit that $\alpha^2_{RP} \rightarrow 0$. Ion pair charge transfer spectra and outer-sphere electron-transfer systems are used to define this limit. One effect of values of $\alpha^2_{RP} \geq 0.03$ is the dramatic attenuation of electron-transfer reorganizational energies, and this effect is examined with respect to the variations in the vibronic contributions of the bpy ligand to the 77 K emission spectra of am(m)ine-polypyridine ruthenium(II) complexes. These contributions of high frequency vibrational modes are manifested in the carefully calibrated near infrared emission spectra as changes in the relative intensities of the vibronic sidebands or in the band shape on the low energy side of the spectrum. These vibronic contributions are most clearly exhibited in empirical reorganizational energy profiles (emreps) based on $\Lambda_x = h\nu_{vib}(\Delta I_{obsd}/I_{max(f)})$, where ΔI_{obsd} is the intensity difference between the observed emission spectrum and the fundamental component. The emreps provide a useful approach for examining the experimental spectral data for contributions of high frequency vibrational modes to the excited state distortion. The respective emreps clearly display the attenuation of the bpy-centered vibronic contributions with the fraction of charge delocalized. The implications for the electron-transfer coordinate in these strongly coupled D/A complexes are considered. Strong electronic coupling between the donor and the acceptor (or between the initial and the product of electron-transfer states) to the ligand that links them can dramatically change the electron-transfer properties of the D/A complex. Work of the Taube group illustrates the variations in H_{RP} that are induced by the bridging ligand. Other effects of strong coupling with the bridging ligand are: (1) reductions of the energy of the D/A electron-transfer absorption band that are roughly proportional to H_{RP}; (2) bridging ligand distortions that alter H_{RP} and also result in contributions of the bridging ligand vibrational modes to the electron-transfer reorganizational energy. The first of these effects is a characteristic of superexchange coupling and the substituted-dipyridyl ligand-bridged $Ru(NH_3)_5^{2+}/Ru(NH_3)_5^{3+}$ complexes (studied by Sutton and Taube) are considered as models. Cyanide-bridged metal complexes are models for the second effect. The entanglement of the nuclear coordinates of the bridging cyanide with H_{RP} (i.e., vibronic coupling, with $H_{RuCr} = H^0_{RuCr} + bQ_{CN}$; where Q_{CN} is the CN bond length and b is a constant) results in anti-kinematic shifts of the ground state CN stretching frequencies of $M(CN)Ru(NH_3)_5$ complexes and in a failure of superexchange coupling in a series of $[\{Ru(NH_3)_5\}_2M(MCL)(CN)_2]^{6+}$ complexes (MCL = a tetraazamacrocyclic ligand). The electron-transfer emissions of these complexes, displayed as emreps indicate that the CN stretch contributes more than 100 cm^{-1} to the overall electron-transfer reorganizational energy in CN-bridged complexes, and implicate a dominant NH stretching mode-mediated nuclear tunneling pathway for back electron-transfer in these complexes. Excited state electron-transfer relaxation by means of NH mediated nuclear tunneling pathways appear to dominate for $\{Cr^{II}(CN)Ru^{III}\} \rightarrow \{Cr^{III}(CN)Ru^{II}\}$ at 77 K, but a more efficient relaxation pathway appears to be important for the am(m)ine-polypyridyl Ru^{II} complexes.

Keywords: Ammine-polypyridine ruthenium(II) complexes; Cyanide-bridged transition metal complexes; Near infrared electron-transfer emission; Superexchange coupling; Vibronic coupling; High-frequency vibronic modes

1. Introduction

The experimental studies of Henry Taube and his associates defined the basic parameters of electron-transfer processes [1–3]. These processes encompass a vast range of phenomena, including fundamental aspects of chemical reactivity and spectroscopy and extending to solar conversion and electronic devices [4]. The theoretical relationships between charge transfer spectroscopy and electron-transfer kinetics was pioneered in Noel Hush's work [5–7], and these relationships were systematically evaluated in Henry Taube's experimental studies [3,8–15]. These relationships have been reviewed in several places [2,3,16–27], and several theoretical models have been proposed to describe aspects of electron-transfer systems [5–7,18,22–24,28–49]. The material emphasized in this article deals with the characteristics and implications of electron-transfer emission spectra of transition metal donor/acceptor (D/A) complexes. These spectra contain a great deal of information about the electron-transfer properties of coordination complexes, and the comparison of spectra for closely related complexes can reveal the changes in properties that accompany configurational mixing in strongly coupled D/A systems. Evaluating such changes in electron-transfer properties implies reference to the properties of otherwise equivalent systems in the limit where configurational mixing (or electronic coupling) approaches zero. The experimentally established properties of useful reference systems that approximate this zero-mixing limit can often be found in the work of the Taube group.

The rate constants for electron-transfer reactions of transition metal complexes span a range of at least 10^{20} [2,21,33,43,50,51]. This range of reactivity can be correlated with the optical electron-transfer absorption bands of ion pairs or of covalently linked complexes, and the molar absorptivities of these absorption bands vary from <1 to more than 10^5 [6,21]. Observable electron-transfer properties of a substrate, such as rate constants and molar absorptivities, can be described in terms of the probability per unit time of the transition from an initial state of the system, designated by a subscript R, to a final state, designated by a subscript P. The transition probabilities are functions of basic physical properties of the D/A system such as the net reaction driving force, the accompanying changes in molecular geometry, and the configurational mixing (or electronic coupling) between the donor and the acceptor [2,3,5,6,21].

The bimolecular, or outer-sphere electron-transfer behaviors of transition metal complexes are generally well described by the semi-classical models of Marcus and Hush [5,6,29–31], for example see [2,16,21,24,28,43,50,52]. These models presume that there is very little configurational mixing between electronic states. It is common to describe the reactants and products potential energy (PE) surfaces in terms of quadratic (or simple harmonic oscillator (SHO)) functions of displacements in the associated nuclear coordinates (or by, at most, only very small deviations from this limit). This is referred to as the weak-coupling limit in this article (it is often called the non-adiabatic limit). To a significant degree, the models for this limit have become the "standard" models of electron-transfer behavior. The deviations of the observed electron-transfer properties of covalently linked complexes from those expected in the weak-coupling limit can often be attributed to the mixing of properties of the linker with the donor and acceptor electron-transfer properties in such a way that the PE surfaces are distorted from the parabolic limit. Systematic studies of linked D/A complexes attempt to determine how D/A configurational mixing alters molecular properties. In order to accomplish this, we reference the properties of the linked system to those of equivalent weakly coupled complexes.

This review will focus on selected spectroscopic probes of the electron-transfer properties of simple, covalently linked transition metal donor-acceptor (D/A) complexes. The principal issues that are considered relate to: (a) how the nuclear coordinates and the donor–acceptor electronic coupling are interrelated for some bridging ligands; (b) how configurational mixing of the bridging ligand with the donor and the acceptor affects the spectroscopic, thermodynamic and kinetic parameters in the linked system; (c) how the highest frequency vibrational modes contribute to the electron-transfer behavior of D/A complexes. Experimental observations on the electron-transfer properties of three classes of complexes that deviate from the weak-coupling limit will be considered here: (a) ruthenium–polypyridyl complexes in which the donor and acceptor are directly linked; (b) cyanide-bridged complexes in which the electronic coupling between the donor and acceptor depends on positions of the atoms in the bridging ligand; (c) some related transition metal D/A complexes with polypyridine linkers.

2. Summary of the expected and observed relationships between spectroscopic and kinetic electron-transfer parameters in the weak-coupling limit

2.1. General considerations and the basis for relating spectroscopic and kinetic Franck-Condon parameters

It is instructive to consider the transition probability in a general and simple form that illustrates the common dependence of the observable electron-transfer properties on molecular-level attributes of the donor and the acceptor in the D/A system [21,53,54],

$$P_{RP} \propto H_{RP}^2 f(\nu_{eff})(FC)_r \tag{1}$$

$$(FC)_r = \sum\nolimits_j F_{j,h}[e^{-\{G_j(r)^2/4RT\chi_s\}}] \tag{2}$$

$$F_{j,h} = \frac{S_h^j e^{-S_h}}{j!} \quad S_h = \frac{\lambda_h}{h\nu_h} \tag{3}$$

Eqs. (1)–(3) are based on SHO models at the weakly coupled limit, and, for spectroscopic transitions, on wave-packet models; H_{RP} (see Section 2.4) is the electronic matrix element; $f(\nu_{eff})$ is an algebraic function that is different for light absorption, light emission and non-radiative relaxation; the solvent reorganizational free energy, χ_s (rather than the reorganizational energy, λ_s) is used for consistency with ΔG^0_{RP}, the high frequency contribution is usually evaluated in terms of an energy contribution; $(FC)_r$ is a "Franck-Condon factor" (note that this is not the Franck-Condon-weighted density of states factor [37]). For simplicity in this description of the basic concepts, only one high frequency vibrational mode (ν_h) is considered here (i.e., Eqs. (2) and (3) represent the vibronic progression in a single normal mode) and any specific effects of solvent structure are ignored. Applications to actual coordination complexes require the inclusion of many additional vibrational modes; this is illustrated in the applications to emission spectroscopy discussed in Section 2.5 below. The transition probability is exponential in $G_j(r)^2$, where,

$$G_j(r) = \Delta G^\circ_{RP} + \chi_s + jh\nu_h + rh\nu_{obsd} \tag{4}$$

The descriptions of light absorption [53,55], light emission [53,55] and non-radiative electron-transfer rate constants [38,53] differ in the last term of Eq. (4) as well as in $f(\nu_{eff})$. The relationships between the spectroscopic and thermal reaction probabilities are given by,

$$\left.\begin{array}{l} r = -1 \text{ (light absorption)} \\ r = 0 \text{ (non-radiative)} \\ r = +1 \text{ (light emission)} \end{array}\right\} \tag{5}$$

Note that ΔG°_{RP} is positive for light absorption and negative for emission. Eqs. (1)–(4) are most nearly correct in the SHO limit where there is very little delocalization of electron density between the donor and acceptor (i.e., where the electron-transfer rate and the intensities of emission and/or absorption approach zero). We refer to this as the "weak-coupling limit."

The exponential factor of $(FC)_r$ tends to dominate Eq. (1), and this feature simplifies much of the discussion. This exponential function is in Gaussian form, and this is the basis for a Gaussian analysis of absorption or emission spectra as well as the Franck-Condon contribution to reaction rates [53,54]. Eqs. (1)–(5) also illustrate fundamental aspects of the interpretation of the vibronic fine structure and the band shapes of the absorption and emission spectral envelopes. As

noted above, real systems require consideration of the contributions of many vibrational modes; furthermore, spectral band shapes are not rigorously Gaussian [56,57], but Gaussian functions have been found to be adequate [54,57,58] except for high-resolution spectra [56,57].

The energy of the absorption maximum corresponds to the maximum value of Eq. (1). Since the nuclei do not move during the optical transition (Franck-Condon principle), there is no entropy change and the energy of the absorption maximum can be expressed in terms of either energy parameters or free energy parameters. For very weak electronic coupling and when high frequency modes do not contribute,

$$h\nu_{max}(\text{abs}) = E^{0'0}_{RP} + \lambda_s + \cdots = |\Delta G^{\circ}_{RP}| + \chi_s + \cdots \quad (6)$$

The emission maximum (for emission of the same electronic state that is populated by absorption, and after vibrational relaxation) is,

$$h\nu_{max}(\text{emis}) = |\Delta G^{\circ}_{RP}| - \chi_s + \cdots \quad (7)$$

An implication of Eq. (6) is that the entropy contribution to the reorganizational free energy, χ_r, cannot generally be neglected. The pressure–volume work for an optical transition is zero, so $|\Delta G^{\circ}_{RP}| = (E^{00}_{RP} - T\Delta S^{\circ}_{RP})$ and $\chi_r = (\lambda_r - T\Delta S_r)$. Thus, the equality in Eq. (6) implies that,

$$\Delta S^{\circ}_{RP} \cong -\Delta S_r \quad (8)$$

Eq. (1) is also the basis for a well-known equation for the bandwidth (full-width at half height, $\Delta\nu_{1/2}$). If there are no other contributions to the bandwidth, the solvent reorganizational energy can be inferred from $\Delta\nu_{1/2}$ for the fundamental component of the CT absorption or emission; assuming a Gaussian band shape [5,6,59],

$$\Delta\nu_{1/2} \cong 4[RT\chi_s\ \ln 2]^{1/2} \quad (9)$$

There are important contributions to the bandwidth in addition to the solvent reorganizational energy. Other contributions to the bandwidths in solutions include: (1) inhomogeneous broadening effects [56], such as result from a distribution of solvent environments and the resulting variations of ΔG^{0}_{RP} and χ_s [21,60]; (2) low frequency molecular vibrational modes and vibrational hot bands. Eq. (9) clearly corresponds to a very simple limit.

When high frequency vibrational modes contribute to the difference in excited- and ground state geometry, then the CT absorption (or emission) envelope will include a series of peaks (vibronic progressions), differing in intensity (an effect of F_j, an expression based on the vibrational overlap integral), but each with the same bandwidth. The vibronic contributions to the CT absorption spectra of transition metal complexes are rarely resolved since most absorption spectra are obtained in ambient solutions, so they are intrinsically broad, and since there are often additional electronic transitions convoluted on the high-energy side of the absorption envelope. The vibronic contributions to emission spectra are more readily identified since the emission spectra most often involve a single electronic excited state relaxing to a single ground electronic state, and these spectra can readily be obtained at low temperatures where the emission bandwidths are smaller and the vibronic components more evident.

However, the emitting states of transition metal complexes generally have spin multiplicities different from those of their ground states. This has implications for the emission energies, and in strongly coupled electron-transfer systems there may also be some differences in the distortions of PE surfaces for the excited states that are initially populated by light absorption and those of the emitting states. The energy difference between the PE minima of a singlet and a triplet excited state with the same orbital population is approximately twice the exchange energy, K_{exch}, if there are no other contributing factors (i.e., in the weakly coupled limit). In general, if two electronic states differ in spin multiplicity, but have the same orbital populations, then the state with the largest spin multiplicity tends to have the lowest energy as a result of the exchange energy contributions. Configurational mixing between electronic states of the same spin multiplicity that are near in energy can alter the sequence of electronic states that differ in spin multiplicity.

For a single contributing high frequency vibrational mode and assuming that the Franck-Condon excited state generated by light absorption, and the emitting state have the same orbital populations but singlet and triplet spin multiplicities, respectively, the energies of the maxima in the absorption and emission spectral components (at j = 0, 1, 2, ...) are determined by the maxima of (FC) and,

$$h\nu_{max}(\text{abs})_j \cong |\Delta G^{\circ}_{RP}| + \chi_s + jh\nu_h + \cdots \quad (10)$$

$$h\nu_{max}(\text{emis})_j \cong |\Delta G^{\circ}_{RP}| - \chi_s - jh\nu_h - 2K_{exch+}\cdots \quad (11)$$

The exchange integral contributions, K_{exch}, to excited state energies can amount to a few thousand wavenumbers for transition metal complexes [61], and they are an issue when comparing absorption and emission energies [60–63]. The resolution of the peaks of a vibronic progression depends on their intensities relative to those of the fundamental (the smaller their relative intensities, the more difficult they are to resolve) and on the relative values of $\Delta\nu_{1/2}$ and $h\nu_h$. When $2\Delta\nu_{1/2} > h\nu_h$, the vibronic components are often difficult to resolve and the spectral band may be significantly distorted (on the high-energy side for absorption and on the low energy side for emission), e.g., see Fig. 1; in this limit molecular modes, as well as solvent modes, can contribute to the effective bandwidth. Most simple interpretations of the bandwidth (e.g., as in Eq. (9) and [6]) are predicated on a Gaussian band shape with contributions only from solvent modes. The resolution of vibronic components is best at low temperature (RT and $\Delta\nu_{1/2}$ small) and in the solid state (where the molecules of interest have a single kind of environment). However, comparisons of series of complexes are most often based on solution spectra both for reasons of convenience and because the spectroscopic parameters obtained in solution are most directly relevant to most observable kinetic properties of a

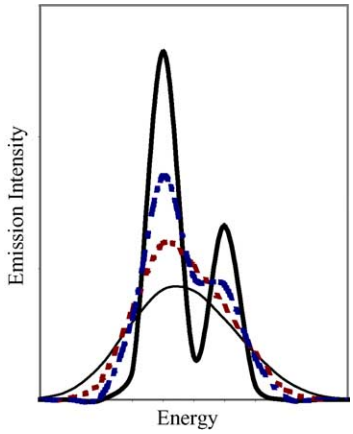

Fig. 1. A qualitative illustration of the dependence on spectral bandwidth of the resolution of a vibronic component whose intensity is half that of the fundamental. For this example it is assumed that $h\nu_{max}(0'0) = 25{,}000\,cm^{-1}$, $h\nu_h = 1000\,cm^{-1}$ and $\Delta\nu_{1/2} = 270$, 420, 600 and $850\,cm^{-1}$, respectively from the top to the bottom curve. Based on Eqs. (1) and (4). The curves have been normalized to have the same integrated intensity.

D/A complex. When the vibronic intensities are small ($S_h < 1$), the intensity of the first vibronic component of a progression, $I_{0'1}$, relative to that of the fundamental, $I_{0'0}$, is given by [56,64],

$$\frac{I_{0'1}}{I_{0'0}} = S_h = \frac{\lambda_h}{h\nu_h} \tag{12}$$

The preceding discussion is formulated in terms of the contributions of excited state distortion (or reorganizational energies) for one quantized molecular high frequency vibrational mode and a continuum of classical solvent modes. Electron-transfer processes in coordination complexes are generally not so simple. Several high frequency vibrational modes are often implicated in the excited state distortion [65–67], and some of the vibrational modes of a complex may be of sufficiently low frequency ($h\nu_l < 4k_BT$) that they cannot be distinguished from the solvent modes under the conditions of a particular experiment. For the set of molecular vibrational modes, $\nu_M = \{\nu_l, \nu_h\}$, that each make a contribution, λ_M, to the overall reorganizational energy, λ_r, the high frequency ($h\nu_h \geq 4\,k_BT$) and low frequency modes ($h\nu_l < 4\,k_BT$) contribute differently to the transition probability; the distinction is based on the sizes of the vibrational quanta relative to k_BT and to significant thermal populations of vibrational excited states. Under ambient conditions ($k_BT \approx 200\,cm^{-1}$) most metal ligand vibrations will behave as low frequency modes and will contribute to the effective bandwidth.

2.2. Specific relationships between spectroscopic and kinetic parameters in electron-transfer systems in the weak-coupling limit

The rate constant for electron-transfer is concisely expressed by [43],

$$k_{et}(b) = K_A\kappa_{el}\nu_{nu}\kappa_{nu} = K_Ak_{et} \tag{13}$$

In Eq. (13), K_A is the equilibrium constant for the outer-sphere association of the donor and acceptor, κ_{el} is the electronic transmission coefficient (the probability that products form once the nuclear configuration of the transition-state is achieved), ν_{nu} is the effective frequency for nuclear motion along the reaction coordinate in the neighborhood of the transition-state, and the nuclear transmission coefficient, κ_{nu}, is the classical exponential function of the activation energy (equivalent to (*FC*)). The arguments of the preceding section correspond to thermally activated electron-transfer in the weakly-coupled limit ($\kappa_{el} < 1$). The effects of strong electronic coupling can only be evaluated with respect to the limit in which the mixing of the donor and acceptor wave functions goes to zero ($H_{RP} = 0$). This limit is called the "diabatic" limit in this article. This limit is experimentally inaccessible; however, κ_{el} is less than unity for most outer-sphere electron-transfer reactions and the relationships described above hold reasonably well [2,21,43,52,68]. For a simple outer-sphere electron-transfer reaction of the type,

$$D + A \rightarrow D^+ + A^- \tag{14}$$

The parameters contributing to (*FC*) may be experimentally inferred from the determinations of the self-exchange rate constants (the asterisk is used to distinguish different molecules) and half wave potentials of the constituent couples,

$$D + {}^*D^+ \rightleftarrows D^+ + {}^*D,\ k_{et}(D^+/D) \tag{15}$$

$$A^- + {}^*A \rightleftarrows A + {}^*A^-,\ k_{et}(A/A^-) \tag{16}$$

$$D^+ + e^{--} \rightleftarrows D,\ E_{1/2}(D^+/D) \tag{17}$$

$$A + e^- \rightleftarrows A^-,\ E_{1/2}(A/A^-) \tag{18}$$

Since $RT\ \ln[k_{et}(\Delta G^\circ_{RP} = 0)/(\kappa_{el}\nu_{nu})] = -\chi_r/4$, the reorganizational free energy for the reaction in Eq. (14) is $\chi_r = 1/2\ [\chi_r(D^+/D) + \chi_r(A/A^-)]$ [30,31], and it is experimentally accessible. Similarly, the free energy change for the electron-transfer in Eq. (14) is $\Delta G^\circ_{RP} = -F\Delta E_{1/2}$, where F is Faraday's constant and $\Delta E_{1/2}(D/A) = [E_{1/2}(A/A^-) - E_{1/2}(D^+/D)]$ (work term corrections have been omitted for simplicity).

The optical transition that is correlated to Eq. (14) is an ion pair charge transfer (IPCT) absorption (the curly brackets represent contact ion pairs) [27,69,70],

$$\{D, A\} + h\nu \rightarrow \{D^+, A^-\} \tag{19}$$

Based on Eq. (6), the IPCT absorption maximum can be represented by (Δw is the electrostatic work term

contribution),

$$h\nu_{\max}(\text{abs}) = -F\Delta E_{1/2}(D/A) + \frac{1}{2}\left[\chi_r(D^+/D) + \chi_r(A/A^-)\right] + \Delta w \quad (20)$$

This relationship provides a very good correlation of the IPCT energy maxima and thermal electron-transfer data for about 30 ion pair couples and about a 5 eV range of optical transition energies (the actual correlation combined independent observations from more than 30 laboratories) [21,69,70]. Almost all of the IPCT absorption bands have molar absorptivities of $<10^3\ M^{-1}\ cm^{-1}$, values of $\kappa_{el} < 1$ and fall in the weakly coupled regime [21]. The relationship between the optical and thermal measurements in this limit is in agreement with Eq. (20) within the quality of the experimental data. This provides the basis for reference systems with respect to which the effects of configurational mixing (or electron delocalization) can be evaluated.

2.3. Simple single mode relationships for the weak-coupling limit

The theoretical models employed in the weakly coupled limit can be classical (e.g., the Marcus theory) [6,29,30,43], semi-classical [38,43] or quantum-mechanical [35,36]. A relatively simple expression for the electron-transfer rate constant that is readily related to Eqs. (1)–(4) is [38,53],

$$k_{et} = \frac{2\pi^2}{h}\frac{{H_{RP}}^2}{(\pi\chi_s k_B T)^{1/2}}(FC)_{r=0} \quad (21)$$

A closely related expression for the electron-transfer absorptivity, obtained from a wave-packet model of the absorption process, is [53,55],

$$\varepsilon_{\nu_m} = \frac{8N\pi^3}{3000h^2 c\nu_m \ln 10}\frac{\eta{H_{RP}}^2(\Delta\mu_{RP})^2}{(4\pi\chi_s k_B T)^{1/2}}(FC)_{r=-1} \quad (22)$$

In Eq. (22), N is the Avagadro's number, η the index of refraction and c the speed of light. This expression depends on the substitution of $H_{RP}\Delta\mu_{RP}/h\nu_m$ for the transition dipole, M_{RP} [53,55,71]. The related expression for the emission intensity is [53,55],

$$I_{\nu_m} = \frac{64\pi^4}{3h^3c^3 \ln 10}\frac{\nu_m\eta^3{H_{PR}}^2(\Delta\mu_{PR})^2}{(4\pi\chi_s k_B T)^{1/2}}(FC)_{r=+1} \quad (23)$$

It should be noted that Eq. (21) is only valid in the weakly coupled limit ($\kappa_{el} < 1$). For ν_{el} an electron hopping frequency in the transition state, κ_{el} can be approximated by,

$$\left[\frac{1}{1 + h\nu_{nu}(\pi\chi_s k_B T)^{1/2}/(2\pi^2 H_{DA}^2)}\right] = \frac{1}{1 + \nu_{nu}/\nu_{el}} \quad (24)$$

Eqs. (22) and (23) are applicable in both the weakly and moderately coupled limits (see discussion below). Eqs. (21)–(23) all assume a SHO model for the molecular vibrations.

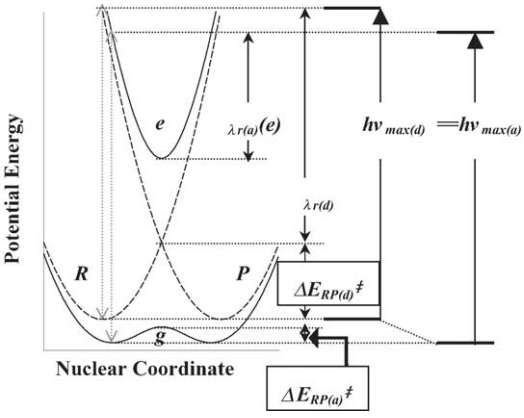

Fig. 2. Qualitative representation of the effects of extensive configurational mixing on the energies for a degenerate ($E_{RP}^{0'0} = 0$) electron-transfer system in the two state limit: (a) owing to the shift of PE minima, the vertical energy differences (light double-headed arrows on the left) at the ground state minima are nearly the same in the diabatic (unmixed; dashed curves) and adiabatic (mixed; solid curves) limits, and $h\nu_{max(d)} = h\nu_{max(a)}$, (b) the activation energy for electron-transfer is smaller in the adiabatic limit, $\Delta E_{RP(a)}^{\neq} < \Delta E_{RP(d)}^{\neq}$, (c) the reorganizational energies are smaller in the adiabatic limit, $\lambda_{r(a)}(e) < \lambda_{r(d)}$, and (d) the reorganizational energies in the adiabatic limit are different for the ground and excited state, $\lambda_{r(a)}(g) \leq \lambda_{r(a)}(e)$.

2.4. Configurational mixing and the electronic matrix element

The configurational mixing in a two state electron-transfer system is represented in terms of reactant (R) and product (P) state electronic wavefunctions (d designates wave functions for the diabatic electronic states) when $E_{RP} > 0$,

$$\psi_R = \frac{\psi_{R(d)} + \alpha_{RP}\psi_{P(d)}}{(1 + \alpha_{RP}^2)^{1/2}} \quad (25)$$

$$\psi_P = \frac{\psi_{P(d)} + \alpha_{PR}\psi_{R(d)}}{(1 + \alpha_{PR}^2)^{1/2}} \quad (26)$$

Note that $\alpha_{RP} = \alpha_{PR}$ when these quantities are evaluated in the coordinates of either the ground or of the excited state PE minimum (or if evaluated at either PE minimum of a self-exchange or mixed valence electron-transfer system with $E_{RP}(0'0) = 0$), but that these quantities are expected to be larger when evaluated at the excited state PE minimum than at the ground state PE minimum of an electron-transfer system if $E_{RP}(0'0) > 0$. The effects of the configurational mixing are to stabilize the ground state, destabilize the excited state and move the PE minima closer together, see Fig. 2. Such configurational mixing affects several of the features of the electron-transfer absorption and emission bands, and it results in an increased rate constant for electron-transfer.

The electronic matrix element, as employed throughout this review, is defined for an appropriate Hamiltonian

operator, $H = H^0 + H' + \cdots$ (where H^0 is the zero order Hamiltonian with respect to which the diabatic states are orthogonal, and H′ is a perturbational Hamiltonian that mixes the diabatic states), with respect to Eqs. (25) and (26),

$$H_{RP} = \langle \psi_R / H' | \psi_P \rangle \cong H^0_{RP} + H^{spx}_{RP} + \cdots \quad (27)$$

Note that Eq. (27) implies that the normalization factors of Eqs. (25) and (26) are implicit in the matrix elements; this is the case for all H_{ij} and α_{ij} quantities in the remainder of this article. The matrix element for the direct overlap of the donor and acceptor wave functions is given by,

$$H^0_{RP} \cong \langle \psi_{R(d)} | H' | \psi_{P(d)} \rangle \quad (28)$$

In Eq. (28), H' is a perturbation Hamiltonian that mixes the electronic state wave functions.

The superexchange contribution, H^{spx}_{RP}, is discussed below. Obviously, the terms that contribute to H_{RP} (Eq. (27)) depend on the definition of the diabatic wave functions. One must be consistent in the choice and use of reference states. Values of the matrix element can be inferred from the deviations of some measured parameter (absorptivity, half-wave potential, attenuation of vibronic band intensity, etc.) from that characteristic of the diabatic limit, usually based on some form of perturbation theory logic. The magnitudes of such deviations increase as a function of the fraction of an electron that is delocalized between donor and acceptor, $\alpha^2_{RP}/(1 + \alpha_{RP})^2$. The most common approaches are based on D/A spectroscopy. The integrated intensity of an electronic absorption band is related to the square of the matrix element; Eq. (22). For a Gaussian-shaped absorption band, this relationship can be expressed as [6,72]

$$H_{RP} \cong \frac{0.0206}{r_{RP}} \left[\frac{(\varepsilon_{max} \Delta\nu_{1/2}) h\nu_{max}}{g_o} \right]^{1/2} \quad (29)$$

In Eq. (29), ε_{max} is the molar absorptivity at the absorption maximum, $\Delta\nu_{1/2}$ is the full-width at half height, $h\nu_{max}$ is the energy of the absorption maximum, g_o is an orbital degeneracy factor (important only for comparisons of systems with different numbers of partly filled orbitals, and usually ignored); r_{RP} is a distance parameter. The distance parameter can be interpreted as the distance between the centers of electron density in the ground and in the excited state [72]. In the diabatic limit (where $\varepsilon_{max} = 0$) r_{RP} can be taken to be the distance between the centers of the donor and acceptor orbitals, d_{DA}; otherwise, it is smaller and not directly measurable; when the only correction arises from electronic delocalization between donor and acceptor and for $\alpha^2_{RP} < 0.1$, $r_{RP} \approx (1 - 2\alpha^2_{RP}) d_{RP}$ (see also Eq. (42) and the comments which follow). Electroabsorption spectroscopy has been used for a less ambiguous approach to inferring the matrix element from electronic absorption spectra [73]; see Section 3.1.

2.5. Vibronic contributions to emission spectra

In general, a large number of vibrational modes are required to describe the distortions of transition metal D/A excited states. Since emission spectra are of particular importance in this article, a more elaborate, multi-mode approach for interpreting emission spectra is included here. Some variation on this approach, rather than Eq. (23), should be used for most complex molecules. Analogous expressions can be generated to describe absorption spectra and rate constants when many vibrational modes contribute to the structural differences between the ground and excited states (or between reactants and products). As noted above, we approximate the vibronic band shapes with Gaussian functions. These ideas can be combined with Eqs. (1), (2) and (23) to model the emission spectrum as described here.

The intensity of the fundamental $\{e, 0'\} \rightarrow \{g, 0\}$ at a frequency, ν_{em}, is constructed as:

$$I_{\nu_m(f)} \cong I_{max(f)}\, e^{-\{[h\nu_{max(f)} - h\nu_m]^2/(\Delta\nu^2_{1/2}/4 \ln 2)\}} \quad (30)$$

The first order vibronic terms are constructed as:

$$I_{\nu_m(0'1)} \cong I_{max(f)} \sum_h \left(\frac{\lambda_h}{h\nu_h} \right) e^{-\{[h\nu_{max(f)} - h\nu_h - h\nu_m]^2/(\Delta\nu^2_{1/2}/4 \ln 2)\}} \quad (31)$$

The second order vibronic terms are constructed as:

$$I_{\nu_m(0'2)} \cong \frac{I_{max(f)}}{2} \sum_i \sum_j \left(\frac{\lambda_i}{h\nu_i} \right) \left(\frac{\lambda_j}{h\nu_j} \right) \times e^{-\{[h\nu_{max(f)} - h\nu_i - h\nu_j - h\nu_m]^2/(\Delta\nu_{1/2}{}^2/4 \ln 2)\}} \quad (32)$$

The third order terms would be constructed as:

$$I_{\nu_m(0'3)} \cong \frac{I_{max(f)}}{6} \sum_i \sum_j \sum_k \left(\frac{\lambda_i}{h\nu_i} \right) \left(\frac{\lambda_j}{h\nu_j} \right) \left(\frac{\lambda_k}{h\nu_k} \right) \times e^{-\{[h\nu_{max(f)} - h\nu_i - h\nu_j - h\nu_k - h\nu_m]^2/(\Delta\nu^2_{1/2}/4 \ln 2)\}} \quad (33)$$

Then the intensity at a frequency ν_m is given by:

$$I_{\nu_m(spec)} \cong I_{\nu_m(f)} + I_{\nu_m(0'1)} + I_{\nu_m(0'2)} + I_{\nu_m(0'3)} + \cdots \quad (34)$$

The emission spectrum is the graphical presentation of $I_{\nu_m(spec)}$ versus ν_m. Note that this is the basis for interpreting the observed spectrum (spec = obsd, below) or for constructing a theoretical spectrum from other information (such as resonance-Raman data; when this is the case, spec = calcd).

2.6. Observations on D/A complexes in the weakly coupled limit; reference systems for the evaluation of the effects of configurational mixing

The general correlation between the optical and thermal properties of ion pairs has been mentioned above and discussed elsewhere [21,69]. An illustrative example is discussed here.

The ferrocyanide/ferricyanide self-exchange reaction, Eq. (35), has been exhaustively studied [74–76].

$$[Fe(CN)_6]^{4-} + [^*Fe(CN)_6]^{3-} \rightleftarrows [^*Fe(CN)_6]^{3-} + [^*Fe(CN)_6]^{4-} \quad (35)$$

This reaction is strongly "catalyzed" by cations, and the uncatalyzed rate constant in aqueous solution (25 °C, I = 0.2 M) is $k_{et}(b)$ = 2.2 × 10^2 M^{-1} s^{-1} [74–76]. In concentrated solutions ([K^+] = 2.5 M, $I \sim$ 10 M and K_A reported to be 0.05 M^{-1}), the $\{[Fe(CN)_6]^{4-}, [Fe(CN)_6]^{3-}\}$ ion pair has been reported to have an absorption maximum at 12.2 × 10^3 cm^{-1} with ε_{max} = 28 cm^{-1} M^{-1} and $\Delta\nu_{1/2}$ = 7.9 × 10^3 cm^{-1} [77]. Based on Eq. (29) (neglecting g), H_{RP} = 116 cm^{-1}. Substitution into Eq. (24) gives κ_{el} = 0.53. This estimate of κ_{el} with $K_A \cong 5 \times 10^{-2}$ M^{-1}, $\nu_{nu} \cong 2 \times 10^{12}$ s^{-1} [68] and assuming that solvent reorganization is the only contribution to χ_r leads to $k_{et}(b)/K_A = k_{et} \approx 4 \times 10^4$ s^{-1}, so that $\Delta G^{\ddagger}_{RP} = \chi_r/4 \cong 3.6 \times 103$ cm^{-1} and $\chi_s(th) \cong 15 \times 10^3$ cm^{-1}. The estimates of $\chi_r(th) \cong 15 \times 10^3$ cm^{-1} and $\chi_r(op) \cong 12.2 \times 10^3$ cm^{-1} are in good agreement.

The bandwidth reported for the $\{[Fe(CN)_6]^{4-}, [Fe(CN)_6]^{3-}\}$ ion pair is about 10^3 cm^{-1} larger than expected based on the observed absorption maximum and Eq. (9). This may indicate that the solutions used contain a distribution of ion pair species, each with a slightly different (not necessarily symmetrical) solvation or distribution of associated cations, resulting in different values of χ_r, ΔG^0_{RP} and/or H_{RP}. The parameters evaluated here indicate that $\alpha^2_{RP} \cong 10^{-4}$ and that there is very little delocalization of electron density in the ground state of the ion pair. Thus, electronic configurational mixing in the ion pair does not significantly modify the properties of the donor and acceptor. This appears to be the general situation for transition metal outer-sphere and ion pair electron-transfer systems [21].

Bimetallic complexes in which the donor and acceptor are linked across aliphatic chains can also fall into the weakly coupled regime. This is illustrated by detailed studies employing the 1,2-*bis*(2,2′ bipyridyl-4′-yl)ethane (bb) linker [78,79]. Three transient absorptions were resolved following photoexcitation of $[(bpy)_2Ru^{II}(bb)Co^{III}(bpy)_2]^{5+}$, with the final step resulting in regeneration of the ground state [78]. These transients were interpreted in terms of the reactions,

$$[(bpy)_2Ru^{II}(bb)Co^{III}(bpy)_2]^{5+} + h\nu \rightarrow^* [(^3MLCT)(bpy)_2Ru(bb)Co^{III}(bpy)_2]^{5+} \quad (36)$$

$$^*[(^3MLCT)(bpy)_2Ru(bb)Co^{III}(bpy)_2]^{5+} \rightarrow [(bpy)_2Ru^{III}(bb^-)Co^{III}(bpy)_2]^{5+} \quad (37)$$

$$^*[(^3MLCT)(bpy)_2Ru(bb)Co^{III}(bpy)_2]^{5+} \rightarrow [(bpy)_2Ru^{II}(bb)Co^{III}(bpy)_2]^{5+} \quad (38)$$

$$[(bpy)_2Ru^{III}(bb^-)Co^{III}(bpy)_2]^{5+} \rightarrow [(bpy)_2Ru^{III}(bb)(^2E)Co^{II}(bpy)_2]^{5+} \quad (39)$$

$$[(bpy)_2Ru^{III}(bb)(^2E)Co^{II}(bpy)_2]^{5+} \rightarrow [(bpy)_2Ru^{III}(bb)(^4T)Co^{II}(bpy)_2]^{5+} \quad (40)$$

$$[(bpy)_2Ru^{III}(bb)(^4T)Co^{II}(bpy)_2]^{5+} \rightarrow [(bpy)_2Ru^{II}(bb)Co^{III}(bpy)_2]^{5+} \quad (41)$$

Thus, it was proposed that photoexcitation of the $[(bpy)_2Ru–]^{2+}$ moiety, Eq. (36), was followed by the hopping of the electron across the bb bridging ligand, Eq. (37), in competition with relaxation to the ground state, Eq. (38), electron-transfer to the doublet (or low spin) excited state of Co(II), Eq. (39), electronic relaxation of the initial Co(II) product excited state, Eq. (40), and back electron-transfer to regenerate the ground state, Eq. (41). The back electron-transfer reaction, Eq. (41), is two to three orders of magnitude slower than expected based on comparison to the respective self-exchange reactions and the measured free energy changes. This appears to be an electronic effect and $\kappa_{el} \sim (10^{-2}–10^{-3})$, and [78] $H_{DA} \sim 8$ cm^{-1} for the spin forbidden process in Eq. (41). Examination of the outer-sphere, back electron-transfer reaction that follows the photoexcitation of $[Ru(bpy)_3]^{2+}$ in the presence of $[Co(bpy)_3]^{3+}$ led to very similar conclusions [80].

3. The effects of appreciable configurational mixing in the two state limit

The ambient charge transfer spectra of transition metal complexes tend to be broad and structureless, and their spectral fittings are not sensitive to the exact choice of parameters (such as solvent reorganizational energies, coupled high frequency vibrational modes and electronic factors) [58]. One expects fittings of ambient electron-transfer rate constant data to be similarly insensitive to the choice of these parameters [58]. It is possible to successfully fit both the ambient spectral and kinetic data for a strongly coupled electron-transfer system in the Marcus inverted region to specific values for the solvent reorganizational energy, the frequency and reorganizational energy of one "average" high frequency distortion mode and an electronic factor in some variation on Eq.

(21) [38,81,82]. These approaches do nicely illustrate the dependence of spectra and rates on each type of parameter. However, such spectral fittings are accomplished by adjusting the values of at least four interdependent parameters, and the physical significance of the numerical values of any such fitted parameters is not clear. This is particularly an issue if one attempts to interpret the values of these parameters or to compare a given parameter for a series of related molecules in order to evaluate the effects of configurational mixing in strongly coupled systems (see additional comments in Sections 3.2.4 and 3.2.5). Nevertheless, it is sometimes possible to combine the observed ambient electronic spectroscopy with data from other types of measurement in order to obtain useful information.

In this section we focus on the metal-to-ligand charge transfer spectroscopy (MLCT) of $[Ru(Am)_{6-2n}(bpy)_n]^{2+}$ complexes (Am = NH_3 or en) as examples of the observable variations in electron-transfer properties attributable to strong electronic coupling. We discuss these complicated systems in terms of the perturbation theory-based deviations from the weakly coupled limit, and Eqs. (21)–(23), that are expected when configurational mixing becomes significant [21,60,62,3].

3.1. Perturbation theory-based expectations

In principle, all of the diabatic electronic states that have the same symmetry should be configurationally mixed. For $E_{ij} > 0$, the mixing coefficients are of the form, $\alpha_{ij} = H_{ij}/E_{ij(d)}$, where H_{ij} is the matrix element coupling the ith and jth diabatic electronic states and $E_{ij(d)}$ is the vertical energy difference between those diabatic electronic states.

In an electron-transfer system, we are concerned with: (a) the direct mixing of donor and acceptor electronic configurations (expressed by H^0_{RP}); (b) any configurational mixings with other electronic states in the complex system that significantly alter the energies and shapes of the ground or excited state PE surfaces and/or the value H_{RP}. For the purpose of experimental studies and comparisons of observations, it is useful to define the "diabatic" donor and acceptor states in terms of the properties of the isolated reductants and oxidants. This definition allows for configurational mixing of the metal with its ligands to be included in the definition of the "diabatic" donor or acceptor state of a coordination complex. When these reactants are assembled for reaction (as in an ion pair or in a bridged D/A complex), the changes in their properties are a measure of the donor/acceptor electronic coupling. Conventional perturbation theory approaches [72] can be used to address the magnitudes and trends of these changes.

Electroabsorption spectroscopy [73] allows the experimental determination of both the difference of the ground and excited state molecular dipole moments ($\Delta\mu_{RP}$) and the electronic transition moment (M_{RP}). These quantities can be directly related to the electronic matrix element [23,73,83],

$$H_{RP} = \frac{|\vec{M}_{RP}|}{[4M^2_{RP} + \Delta\mu^2_{RP}]^{1/2}} E_{RP} \quad (42)$$

The electroabsorption technique has been used primarily for covalently linked donor-acceptor complexes that are in the very strongly coupled regime (i.e., for MLCT absorption spectra) [73]. Eq. (42) can be rearranged to give $M^2_{RP}(1 - 4\alpha^2_{RP}) = \Delta\mu^2_{RP}H^2_{RP}/h\nu^2_m$, and this suggests that the substitution of $(\Delta\mu^2_{RP}H^2_{RP}/h\nu^2_m)$ for M^2_{RP} involved in the derivation of Eqs. (22) and (23) [53] is only valid when $\alpha^2_{RP} < 0.1$. The behavior for larger values of α^2_{RP} is not well described by these functions. One expects $\Delta\mu_{RP}$ to decrease as the amount of charge delocalized increases. With sufficient charge delocalization, the electronic transition should become more like a $\pi \rightarrow \pi^*$ transition than a MLCT transition [84], and this is a plausible interpretation of the $(1 - 4\alpha^2_{RP})$ factor in the rearranged Eq. (42).

The energies of the ground state absorption maxima for degenerate systems are independent of the extent of configurational mixing in the range $0 < 2H^0_{RP} <\sim (\lambda_r/4 - 2k_BT)$ in the two state limit. For non-degenerate systems the absorption band energies do change with the extent of configurational mixing. While the energies of the optical electron-transfer transitions may sometimes be independent of configurational mixing in this limit, the absorption and emission bandwidths are expected to decrease appreciably with increases in configurational mixing. The reorganizational energy, λ_r, corresponding to an electronic emission is the energy of the final state with its nuclear coordinates in the configuration of the initial state PE minimum minus the energy of the final state at its PE minimum. Configurational mixing decreases the difference in these PE minima and it results in changes of shape of the adiabatic PE surfaces relative to the diabatic (or unmixed) PE surfaces. As a result, λ_r decreases as configurational mixing between these states increases, and this can be evaluated by means of perturbation theory arguments [60,63]; for $\alpha^2_{RP} < 0.1$,

$$\lambda_{r(a)} \cong \lambda_{r(d)}(1 - 4\alpha^2_{RP}) \quad (43)$$

Eq. (43) can be interpreted in terms of the attenuation of reorganizational energies that accompany the transfer a fraction of electron density, α^2_{RP}, from the donor to the acceptor. Hush [5] and Matyushov et al. [41,85,86] have defined a delocalization parameter based on the solvent response to changes in ionic charge (and in terms adiabatic absorption parameters) to obtain an expression very closely related to Eq. (43) for the attenuation of λ_s. As a consequence, when configurational mixing is important Eq. (9) should be rewritten

$$\Delta\nu_{1/2(a)} \cong 4[RT\lambda_{s(d)}(1 - 4\alpha^2_{RP}) \ln 2]^{1/2} \quad (44)$$

Eq. (43) can be interpreted as a perturbation theory-based statement that the amount of excited state distortion decreases as the amount of electron density delocalized between the

two states increases, and it can be obtained for a general distortion coordinate (in Eq. (43) designated by the subscript r). This implies that there should be a corresponding attenuation of the relative intensities of the vibronic side bands of the coupled high frequency vibrational modes with increases in configurational mixing. Conversely, if this argument is correct, the attenuation in the vibronic sidebands could be developed into a simple and experimentally accessible measure of the extent of configurational mixing. The interpretation of the relative intensities of the vibronic sidebands that originate from the contributions of high frequency vibrational modes should be less susceptible to ambiguities than the interpretation of bandwidth: the issues related to any contributions from variations in solvent/ligand interactions or in the distributions of solvates should be much less important. These points are being investigated, and the current experimental observations are summarized below.

Since the transition probability increases as H_{RP}^2 (Eq. (1)), one expects that the electron-transfer absorption bandwidth should decrease as the absorptivity of the band increases for CT absorption bands of similar energies; thus, for $4\alpha_{RP}^2 \ll 1$, $\Delta\nu_{1/2(a)} \cong \Delta\nu_{1/2(d)}(1 - 2\alpha_{RP}^2) \propto (1 - 2\varepsilon_{max}(RP)/\varepsilon_{max}^0)$, where ε_{max}^0 is the absorptivity of an equivalent fully allowed transition. Finally, if the emission is from an electronic state that differs in spin multiplicity from the ground state, then the vertical energy differences and possibly the electronic matrix elements will be different for the configurational mixing that alters the respective PE surfaces near their PE minima. If the matrix elements were to be the same (as in fluorescence), then $\alpha_{RP(G)} < \alpha_{PR(E)}$ (G and E designate parameters evaluated in the coordinates of the ground state and excited state PE minima, respectively) and the bandwidth and vibronic component intensities should be more attenuated in emission than in absorption spectra. For emissive transitions between states that differ in spin multiplicity (as in phosphorescence spectra), the ground state and excited state PE surfaces may be distorted differently as a consequence of their mixing with states of different spin multiplicity (e.g., singlet and triplet states, respectively); this may lead to different changes in the energies and coordinates of the PE minima than when the ground and excited states are directly mixed. Some of the issues that arise can be addressed by considering the mixing of a ground state with singlet spin multiplicity with a triplet excited state to be effected by spin-orbit coupling. In this approximation, the effective matrix element for the coupling between the triplet excited state and the singlet ground state can be represented as $H_{PR} \approx (H_{SO}/E_{ST})H_{RP}$, and if the spin-orbit matrix element, H_{SO}, is small compared to the vertical singlet-triplet excited state energy difference, $E_{ST} \cong 2K_{exch}$, then $\alpha_{PR} < \alpha_{RP}$. In general, for a spin-forbidden emission, and for $(\alpha_{RP}^2 + \alpha_{PR}^2) < 0.1$ Eq. (43) becomes [63],

$$\lambda_{r(a)} \cong \lambda_{r(d)}(1 - 2\alpha_{RP}^2 - 2\alpha_{PR}^2) \tag{45}$$

Eq. (45) distinguishes between possible differences in the effects of configurational mixing of the ground and the excited states.

Configurational mixing results in appreciably faster electron-transfer reaction rates than observed in the weakly coupled limit. For strongly coupled systems, Eq. (21) can be put in the form,

$$k_{et} \approx (\nu_{nu}\kappa_{nu})_d f_{ad} \tag{46}$$

where the nuclear frequency and Franck-Condon factors, $(\nu_{nu}\kappa_{nu})_d$, are evaluated with respect to the diabatic (SHO) limit, and for the two state model the adiabatic correction factor is approximately given by $f_{ad} \cong \exp(H_{RP}/k_BT)$.

Finally, Eq. (20) needs to be modified in the strong coupling limit since Eq. (14) does not describe the photochemical process when the donor and acceptor are linked [26,60],

$$D(L)A + h\nu \rightarrow D^+(L)A^- \tag{47}$$

The corresponding electrochemical processes are,

$$D^+(L)A + e^- \rightleftarrows D(L)A,\ E_{1/2}(D) \tag{48}$$

$$D(L)A + e^- \rightleftarrows D(L)A^-,\ E_{1/2}(A) \tag{49}$$

The electrochemical and photochemical processes are related by means of the one-electron equilibrium,

$$D^+(L)A^- + D(L)A \rightleftarrows D^+(L)A + D(L)A^-,\ K_{DA} \tag{50}$$

If the difference in stabilization from configurational mixing between the ground [D(L)A] and excited [$D^+(L)A^-$] electronic states, evaluated at their respective PE minima, is $(\varepsilon_s - \varepsilon_d) \approx -2\alpha_{RP}^2\lambda_{r(a)}$, then [60],

$$RT\ \ln\ K_{DA} \approx 2\alpha_{RP}^2\lambda_{r(a)} + RT\ \ln\ K_{el} + \Delta K_{exch} \tag{51}$$

where K_{el} is an electrostatic term and ΔK_{exch} represents the net exchange energy difference summed over all the species. Combining Eq. (51) with Eq. (20) gives [60],

$$\begin{aligned} h\nu_{max} &= [E_{1/2}(A) - E_{1/2}(D)] + RT\ \ln\ K_{DA} + \chi_r + \Delta w \\ &\approx F\Delta E_{1/2}(A/D) + \chi_{r(d)}(1 - 2\alpha_{RP}^2) + RTK_{el} \\ &\quad + \Delta K_{exch} + \cdots \end{aligned} \tag{52}$$

Eqs. (38)–(41), (51) and (52) contain only the lowest order of correction terms. When electronic delocalization is large (e.g., for $\alpha_{RP}^2 >\sim 0.1$), higher order terms become important [60,62,63]. Some of these equations are probably applicable even when the two state model is not; hence, the use of H_{RP} rather than H_{RP}^0. Most strongly coupled electron-transfer systems involve covalently linked donors and acceptors; these are discussed briefly in Section 5.

3.2. Examples of strongly coupled D/A complexes in the two state limit: Ru^{II}–polypyridyl complexes

The $[L_4Ru^{II}bpy]^{2+}$ complexes (L = an am(m)ine or bpy/2) form a simple class of D/A complexes in which the electronic coupling between the donor and acceptor (Ru^{II} and bpy, respectively, in the ground state) is very strong. The values of H_{RP}, based on electroabsorption spectroscopy [87], are reported to be $10.5 \times 10^3\,cm^{-1}$ for $[Ru(NH_3)_5py]^{2+}$. Estimates of H_{RP} for Ru^{II}/(2,2′-bipyridine) complexes (based on absorption spectra and electrochemical measurements) are similarly large (approximately $7 \times 10^3\,cm^{-1}$) [60]. These are among the largest electronic matrix elements reported for D/A complexes. Thus, the observed variations in D/A properties of Ru^{II}-polypyridyl-am(m)ine complexes are examples of the effects of significant, but variable (through variations in E_{RP}), configurational mixing.

3.2.1. Zero point energies

We have used a calibrated InGaAs array detector to extend the range of known emission spectra of Ru^{II}–polypyridyl-am(m)ine complexes to include the spectra of tetraammine complexes [88,89]. The most studied member of the $[Ru(NH_3)_{6-2n}(bpy)_n]^{2+}$ series of complexes is $[Ru(bpy)_3]^{2+}$ [28,90–92]. We have used resonance-Raman (r-R) data obtained for this complex [66] to fit the broad, structureless ambient emission spectrum obtained in a 1:1 DMSO:water solution [89]. The r-R data require a fundamental component whose intensity is about 60% of that obtained from a Grams32 fit of the emission spectrum; the changes in energy and bandwidth of the fundamental were relatively minor for this fit, but the Gaussian fits of the ambient spectra have proved to be difficult to independently reproduce and they have to be regarded as very uncertain. The energy of the fundamental component obtained with the best fit of the r-R data is $h\nu_{max(f)} = 16{,}530\,cm^{-1}$ in excellent agreement with the value of $16{,}500 \pm 400\,cm^{-1}$ obtained from photoacoustic microcalorimetry [93,94].

The 77 K emission spectra exhibit a dominant high-energy component that is mostly (≥70%) fit by a single Gaussian component [60,62,63,89]. The maxima of these components provide plausible estimates of $E_{RP}^{0'0}$. The resonance-Raman spectra of $[Ru(bpy)_3]^{2+}$ [66] and of $[Ru(NH_3)_4(bpy)]^{2+}$ [65] imply that the vibronic contributions to their spectra are relatively small [60] and that the fundamental is the dominant contribution to the high-energy component of the 77 K emission [89]; see Fig. 3. In generating the fits of the resonance-Raman data shown in Fig. 3, we have substituted the values of $h\nu_h$ and λ_h determined from the resonance-Raman spectra into Eqs. (31) and (32), and combined the resulting contributions with Gaussian components representing the fundamental, $I_f(\nu_{em})$ (obtained in the Gaussian fit of the observed emission spectrum using Grams32), in order to construct emission spectra using Eq. (34). The value of $I_f(max)$ was decreased (usually 15–20%) so that the sum of the contributions of all components matched the intensity of the observed spectrum as closely as possible; the values $h\nu_{max(f)}$ and $\Delta\nu_{1/2}$ were generally adjusted slightly (≤|5%|) in order to optimize the fit of the resonance-Raman data. In fitting the resonance-Raman data, we have omitted third and higher order terms. Note that the lower energy "band" of the 77 K emission spectrum of $[Ru(bpy)_3]^{2+}$ is relatively broad because it is the convolution of contributions from several vibronic components.

It has often been noted that the absorption and emission energies of these complexes vary in the same order as the differences of the half-wave potentials for oxidation of the metal and reduction of the polypyridyl ligand, e.g., see [26]. This is illustrated in Fig. 4 for the absorption maxima of a few complexes (the details are summarized in Table 1 and in [60]). These correlations are useful in the assignment of observed electronic transitions, but their detailed interpretation in terms of electron-transfer parameters for systems with a great deal of configurational mixing is not simple; e.g., see Eq. (47). In this discussion, we treat the correlation only as a useful illustration of the effects of variations in several key parameters.

As is noted above, the observed absorption and emission maxima depend on the energy differences between the PE minima of the ground and excited states ($E_{RP}^{0'0} = h\nu_{max(f)}$), the electron-transfer reorganizational parame-

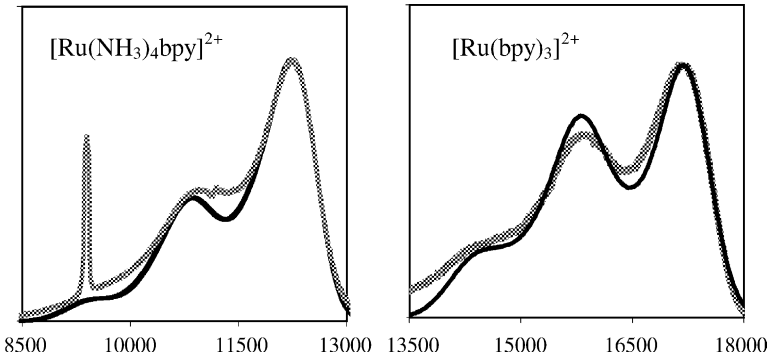

Fig. 3. Comparison of observed emission spectra [89] (thick, dotted line) and spectra constructed from reported resonance-Raman data (solid lines) [65,66] and the fundamental obtained from a Gaussian deconvolution of the 77 K emission spectra in butyronitrile. Eqs. (30)–(32) and (33). Left, $[Ru(NH_3)_4bpy]^{2+}$; right, $[Ru(bpy)_3]^2$.

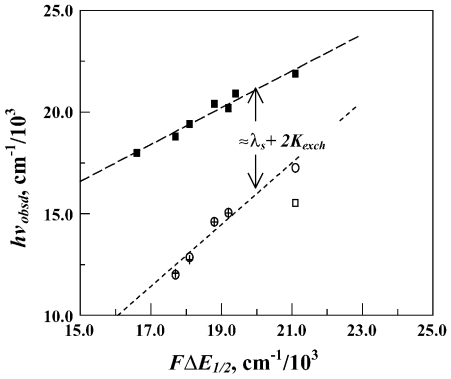

Fig. 4. The relationships between optical transition energies and half-wave potentials for $[Ru(PP)_n(Am)_{6-2n}]^{2+}$ complexes. The halfwave potentials were determined in acetonitrile. Lowest energy absorption maxima, upper set, in water or DMSO/water (filled squares); $E^{0'0}$ from Gaussian deconvolution of 77 K emission spectra, lower set, in DMSO/water (open circles) and the am(m)ine deuterated complexes in DMSO/D_2O (crosses). The value of $E^{0'0}$ for $[Ru(bpy)_3]^{2+}$, open square, is from the resonance-Raman modeling of the ambient emission in DMSO/water. The least squares lines have slopes of 0.90 ± 0.08 (upper; dashed) and 1.5 ± 0.2 (lower for 77 K; dotted) and intercepts of $(3 \pm 1) \times 10^3$ cm^{-1} (upper) and $-(14 \pm 4) \times 10^3$ cm^{-1} (lower; 77 K only). Data from Table 1 and [60].

ters and exchange energy contributions (defined here as the difference between the energies of the PE minima of the MLCT singlet and triplet states with the same orbital occupation). The zero point energy differences are expected to decrease with $F\Delta E_{1/2}$ through the series of complexes. On the other hand, the values of $\lambda_{s(d)}$ and the exchange energies are expected to increase systematically through this series of complexes. Based on our fitting [89] of the resonance-Raman data [66] to the ambient and 77 K emission spectra of $[Ru(bpy)_3]^{2+}$, the energies of the fundamental components are only 700–1000 cm^{-1} smaller in fluid than in frozen solutions. The difference between the energy of fundamental component of the emission and the energy of the absorption maximum for any specific complex is approximately $(\lambda_s + 2K_{exch})$ in ambient solutions. The differences between $h\nu_{max}$(abs; 300 K) and $h\nu_{max(0'0)}$(em) in 77 K frozen solutions clearly increases from $[Ru(bpy)_3]^{2+}$ to $[Ru(NH_3)_4bpy]^{2+}$, the high and low energy extremes, respectively, of Fig. 4, qualitatively in accord with expectation [60–63] (see Eq. (52)). The values of $F\,\Delta E_{1/2}$ depend on energy and entropy changes for the one electron oxidation and the one electron reduction of the D/A complex, and these quantities may not be the same as for the optical transition.

The values found for $E_{RP}{}^{0'0}$ from the 77 K emission spectra vary systematically with $F\,\Delta E_{1/2}$; however the slope of about 1.5 for the correlation in Fig. 4 is larger than expected based on a 1:1 correspondence. Much of this deviation from a unitary slope must originate from the systematic increase of K_{exch} as $E_{RP}{}^{0'0}$ decreases. For example, Lever and Gorelsky [61] have used a ZINDO approach to estimate that, $2K_{exch}$ = 1460 and 4160 cm^{-1} for $[Ru(bpy)_3]^{2+}$ and $[Ru(NH_3)_4(bpy)]^{2+}$, respectively; values this large would certainly be sufficient to account for the differences in the slopes of the correlations of $h\nu_{max(abs)}$ and $E_{RP}{}^{0'0}$ with $F\,\Delta E_{1/2}$ in Fig. 4. Unfortunately the ambient spectra of the complexes considered here are broad and largely unstructured, and a meaningful estimate of $E_{RP}{}^{0'0}$ can be obtained only for $[Ru(bpy)_3]^{2+}$ (from the combination of the emission spectral data with resonance-Raman data or from photoacoustic microcalorimetry).

Table 1
Electronic absorption and emission spectral data for $[Ru(Am)_{6-2n}(bpy)_n]^{2+}$ complexes[a]

Ru^{II} complex [ligands]	$h\nu_{max}$(abs)	$h\nu_{max}$(em), 298 K	$h\nu_{max}$(em), 77 K	$h\nu_{max}$(f), [$\Delta\nu_{1/2}$],[b] 77 K {$h\nu_{max}$(f), [$\Delta\nu_{1/2}$], 298 K}	$\lambda_x(\nu_x)$, 77 K	λ_x(NH), 77 K	k_{nr} (μs^{-1}),77K {k_{nr} (μs^{-1}), 298 K}
$[(bpy)_3]$	21.9(d/w)	15.98(d/w)	17.15(d/w)	17.26 [0.68] (d/w) {16.53[1.64](d/w)}[c]	1.17(1.56) (d/w)		0.23(d/w) {1.1(d/w)}
		16.24(bun)	17.26(bun)	17.34[0.66](bun)	1.02(1.57)(bun)		
$[(en)(bpy)_2]$	20.2(d/w)	13.97(d/w)	14.9(d/w)	15.05 [0.70] (d/w)	1.10(1.47)(d/w)	0.025	1.3(d/w) {12.3(d/w)}
	20.4(bun)	14.35(bun)	15.0(bun)	15.15[0.66](bun)	0.91(1.50)(bun)		0.69(bun) {10.2(bun)}
$[(NH_3)_2(bpy)_2]$	20.4(d/w)	13.52(d/w)	14.3(d/w)	14.61 [0.83] (d/w)	0.95(1.51)(d/w)	0.03	2.9(d/w) {25(d/w)}
	20.2(bun)	13.98(bun)	14.6(bun)	14.69[0.78](bun)	0.90(1.52)(bun)		1.7(bun) {14.5(bun)}
$[(en)_2(bpy)]$	19.1(d/w)	–	12.5(d/w)	12.86 [0.90] (d/w)	0.91(1.41)(d/w)	0.02	26(d/w) 9.5(bun)
	19.2(bun)	–	12.9(bun)	12.99[0.77](bun)	0.85(1.41)(bun)		
$[(NH_3)_4(bpy)]$	18.8(d/w)	–	11.8(d/w)	12.00 [1.15] (d/w)	0.78(1.50)(d/w)	0.027	39(d/w) 22(bun)
	19.0(bun)	–	12.2(bun)	12.42 [0.71](bun)	0.74(1.54)(bun)		
$[(d_4\text{-en})(bpy)_2]$	20.3(d/w)	14.0(d/w)	14.9(d/w)	15.04 [0.71] (d/w)	1.13(1.47)(d/w)		0.66(d/w) {6.2(d/w)}
	20.4(bun)	14.5(bun)	15.0(bun)	15.17[0.76] (bun)	0.77(1.47)(bun)		0.41(bun) {9.0(bun)}
$[(ND_3)_2(bpy)_2]$	20.3(d/w)	13.7(d/w)	14.4(d/w)	14.60 [0.92] (d/w)	0.94(1.51)(d/w)		1.3(d/w) {13.7(d/w)}
	20.3(bun)	14.1(bun)	14.5(bun)	14.62 [0.86] (bun)	1.01(1.49)(bun)		1.1(bun) {13(bun)}
$[(d_4\text{-en})_2(bpy)]$	19.0(d/w)	–	12.6(d/w)	12.73 [0.92] (d/w)	0.88(1.36)(d/w)		8.4(d/w) {*nd*(d/w)}
	19.2(bun)	–	12.9(bun)	12.98 [0.84](bun)	0.82(1.38)(bun)		5.1(bun) {41(bun)}
$[(ND_3)_4(bpy)]$	18.9(d/w)	–	11.9(d/w)	12.06 [1.20] (d/w)	0.78(1.50) (d/w)		13(d/w) {*nd*(d/w)}
	19.2(bun)	–	12.2(bun)	12.41 [0.93] (bun)	0.79(1.51)(bun)		12(bun) {*nd*(bun)}

[a] Data from [60,89]. All energies in cm^{-1}/10^3. D/W = 1:1: DMSO/water; bun = butyronitrile.
[b] Fundamental components based on Grams32 deconvolutions except as indicated.
[c] Fundamental component based on fit of resonance-Raman data.

3.2.2. Solvent reorganizational energies

Differences in solvent reorganizational energy, λ_s, also contribute to correlations such as in Fig. 4. However, the size of these differences is not easily estimated since the effective charge transfer distance is necessarily smaller than the mean radii of the complexes. The values of $\Delta\nu_{1/2}$ in 77 K glasses are small; they increase in the expected order in DMSO/water glasses, but they are nearly constant in butyronitrile. Factors other than reorganizational energies can make significant contributions to the bandwidths in frozen solutions, and at this time it is not clear that the dominant contribution to the emission bandwidths of these complexes arise from solvent reorganizational energy.

3.2.3. Vibronic contributions and their attenuation; some general considerations

We have used the variations in the observed envelope of high-frequency vibronic contributions (at about 1500 cm^{-1}) to evaluate the issue of the extent of attenuation of excited state distortion with electron delocalization. The resonance-Raman data [65,66] imply that most of the vibronic contributions in the 1500 cm^{-1} region are from the contributions of first order components of bipyridine distortion modes [89]. A correlation with the amplitudes of these contributions through the series of $[Ru(Am)_{6-2n}(bpy)_n]^{2+}$ complexes assumes that the emitting excited states differ only in the different fractions of electron density delocalized in each complex, and that the variations in distortion are similar in all of the molecular distortion modes. Before we address the issue of attenuation in the context of emission spectra, it is necessary to consider other information about the high frequency vibronic contributions.

Very low temperature spectroscopic studies of $[Ru(bpy)_3]^{2+}$ [67], and the resonance-Raman spectra of $[Ru(bpy)_3]^{2+}$ [66] and $[Ru(NH_3)_4(bpy)]^{2+}$ [65] have demonstrated that there are a large number of molecular distortion modes in these complexes, see Table 2. If the electronic transition in each case corresponds to a $\{Ru^{III},bpy^-\} \rightarrow \{Ru^{II},bpy\}$ transition, then one expects the same bpy-centered vibrational modes to be correlated to the MLCT transition for each complex, and Eqs. (12) and (45) predict that the ratio of the intensities of these modes for the two complexes is a constant that can be correlated to the electron density delocalized. The resonance-Raman data summarized in Table 2 indicates that the intensities are not the same for all of the detected vibrational modes of these complexes. That the intensity ratios for the same vibrational modes vary over a wide range has been noted previously [58]. The resonance-Raman spectrum probes the Franck-Condon excited state [58], and according to the Franck-Condon principle, this excited state and the ground state must have the same nuclear coordinates and symmetry. This corresponds to D_3 and C_{2v} symmetry, respectively for $[Ru(bpy)_3]^{2+}$ and $[Ru(NH_3)_4(bpy)]^{2+}$. This difference in symmetry necessarily corresponds to differences in the Franck-Condon excited state structure.

Some insight into the MLCT excited states of $[Ru(bpy)_3]^{2+}$ can be based on the symmetries of the $d\pi$ donor orbitals of Ru and the symmetries of the bpy acceptor orbitals adapted to the D_3 point group (e.g., see [95]). The $d\pi$ orbitals have a_2 and e symmetry. A simple construction of the acceptor orbitals is based on the LUMO of a single bpy (b representation in the C_2 site symmetry of the ligand) and the symmetry adapted (see [96]) π^* acceptor orbitals have a_2 and e symmetries. A simple angular overlap argument suggests that the highest energy donor orbitals have $d\pi(a_2)$ symmetry; however, the MLCT state with the $\{d\pi(a_2), \pi^*(a_2)\}$ electronic configuration is dipole forbidden and the state with the $\{d\pi(a_2), \pi^*(e)\}$ configuration is expected to have poor donor orbital/acceptor orbital overlap and to be only weakly

Table 2
Resonance-Raman parameters for $[Ru(bpy)_3]^{2+}$ and $[Ru(NH_3)_4bpy]^{2+}$

For $[Ru(bpy)_3]^{2+}$				For $[Ru(NH_3)_4bpy]^{2+}$				S(B)/S(A)[c]
ν_i, cm^{-1}[a,b]	Δ_i	λ_i, cm^{-1}	$S_i(B)$	ν_i, cm^{-1}[c]	Δ_i	λ_i cm^{-1}	S_i(a)	
1608	0.31	77	0.048	1605	0.38	116	0.072	0.68
1563	0.47	171	0.110	1548	0.36	101	0.065	1.69
1491	0.73	397	0.266	1481	0.55	224	0.151	1.76
1320	0.56	207	0.157	1331	0.41	111	0.084	1.87
1276	0.36	83	0.065					
1264	0.09	5	0.004	1260	0.15	14	0.011	0.36
1176	0.48	135	0.115	1172	0.30	53	0.045	2.55
1110	0.16	14	0.013					
1067	0.10	5	0.005					
1043	0.16	13	0.013	1027	0.32	52	0.051	0.25
766	0.14	8	0.010					
668	0.75	188	0.281	667	0.62	128	0.192	1.46
				456	0.27	17	0.036	
370	0.44	37	0.10	376	0.81	123	0.328	0.306
283	0.50	35	0.125	248	0.46	26	0.106	1.18

[a] [66].
[b] [65].
[c] Ratio of relative, first order vibronic intensities.

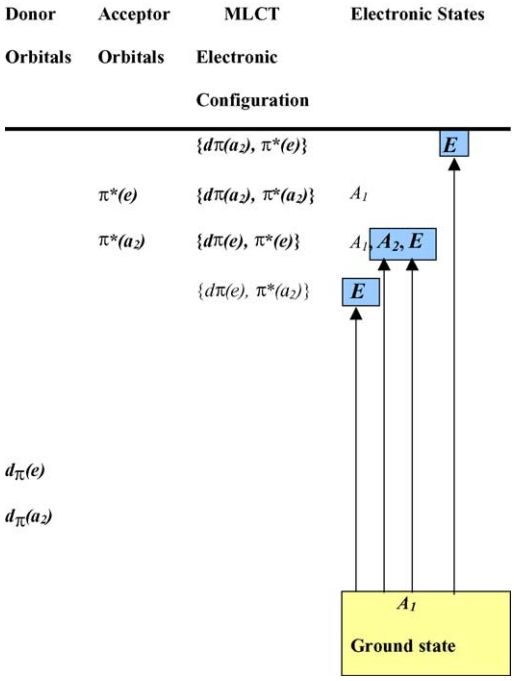

Fig. 5. Electronic configurations and symmetries of the MLCT excited states of $[Ru(bpy)_3]^{2+}$ in D_3 symmetry. Overall energies are assumed to increase from bottom to top, but the relative energies of the different donor orbitals, of the different acceptor orbitals and of the various MLCT excited states are not known. The ligand centered π* acceptor orbital symmetries are constructed by symmetry adaptation of the three equivalent bpy LUMOs (b symmetry in the C_2 point group). The effects of spin-orbit coupling are not considered. The dipole allowed transitions are indicated by the vertical arrows, bold characters and highlighted boxes.

absorbing. Electronic transitions to states with the $\{d\pi(e)^3, \pi^*(a_2)\}$ and $\{d\pi(e)^3, \pi^*(e)\}$ configurations are expected to dominate the absorption. The corresponding MLCT excited states have (E) and ($A_1 + A_2 + E$) symmetries, respectively, and the $A_1 \rightarrow A_2$ and $A_1 \rightarrow E$ MLCT transitions are dipole allowed. The dipole allowed Franck-Condon excited states are not totally symmetric. For the exited states deriving from the $\{d\pi(e)^3, \pi^*(e)\}$ electronic configurations, the acceptor orbitals are approximately of the form (subscripts a, b and c designate the different bpy ligands),

$$\varphi(e_1) \approx \frac{2 \times \pi^*_a - \pi^*_b - \pi^*_c}{(6)^{1/2}} \quad (53)$$

$$\varphi(e_2) \approx \frac{\pi^*_b - \pi^*_c}{(2)^{1/2}} \quad (54)$$

These arguments are summarized in Fig. 5. Since the Franck-Condon excited state of $[Ru(bpy)_3]^{2+}$ must be consistent with the D_3 symmetry, and this symmetry requires acceptor orbitals "delocalized" over the bpy ligands, it is likely that the distortions in some of the vibrational modes are different in this complex and $[Ru(NH_3)_4bpy]^{2+}$.

Overall, the average of the resonance-Raman-based reorganizational energies of the vibronic components is larger for $[Ru(bpy)_3]^{2+}$ than for $[Ru(NH_3)_4(bpy)]^{2+}$ in the 1100–1700 cm^{-1} region, qualitatively as expected based on Eq. (45) and the larger mixing coefficient implied by the lower energy absorption of the latter. However, the opposite ordering is observed for three of the seven common resonance-Raman frequencies in this region, and this suggests different excited state distortions for the two complexes.

McCusker has reported femtosecond absorption anisotropy experiments that indicate that the D_3 ("delocalized", as discussed in the preceding paragraph) symmetry of the Franck-Condon excited state of $[Ru(bpy)_3]^{2+}$ relaxes to a "localized" C_2 symmetry in ambient acetonitrile solutions in about 60 fs [97]. The time required for this apparent localization of the charge on one bpy ligand appears to be correlated with the inertial properties of the solvent [97]. In the limit that the environment cannot rearrange to accommodate the difference in ground and excited state charge distribution, it is possible that the excited state cannot relax to a localized electronic configuration. Thus, the very low temperature, doped single crystal emission of $[Ru(bpy)_3]^{2+}$ has been interpreted in terms of a D_3 MLCT excited state symmetry [67]. Obviously, low temperature glasses fall between these regimes, and there has to be some concern about whether the solvent can rearrange to accommodate the localized (C_2) charge distribution. It is to be noted that a large amount of energy, 4000–5000 cm^{-1} for the complexes considered here, must be deposited in the solvent matrix when the Franck-Condon excited state relaxes to the emitting state. Since heat diffusion is relatively slow, the solvent molecules nearest the electronically excited molecule may be "hot" long enough to rearrange to at least partly stabilize the localized electronic configuration. We will assume that the emitting MLCT states of all the bpy complexes have a localized (C_2) electronic configuration.

3.2.4. Vibronic contributions evaluated in terms of a single "average frequency" distortion mode

Owing to the significant bandwidths and to the relatively small excited state distortions, the vibronic structure is not fully resolved in the 77 K CT emission spectra of most transition metal D/A complexes. In most cases the emission bands are broadened on the low energy side, consistent with the expected vibronic contributions; in a few cases there is some apparent vibronic structure. Such spectra have been successfully fit to an electronic factor, specific values for the solvent reorganizational energy, the frequency and reorganizational energy of one "average" high frequency distortion mode in a variation of Eq. (21) [38,81,82]. We consider aspects of the application of such approaches to the 77 K emission spectra in this section.

The envelope of the vibronic contributions is readily obtained by subtracting the intensity contributions of the fundamental component from the observed emission spectrum. This is illustrated for $[Ru(bpy)_3]^{2+}$ in the middle of Fig. 6 (the difference spectrum is normalized by dividing by the maximum intensity of the fundamental from the Gaussian

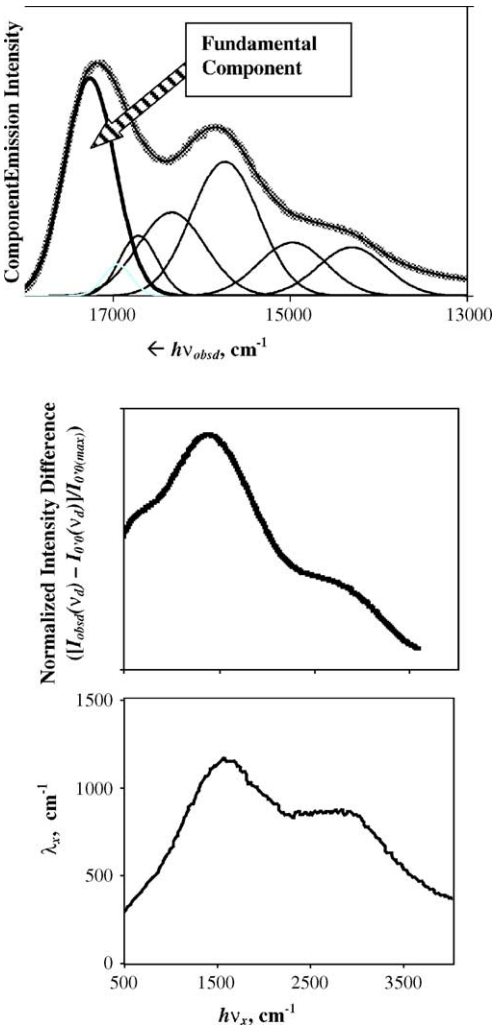

Fig. 6. Emission spectrum (top), difference spectrum (middle) and emrep (bottom) for $[Ru(bpy)_3]^{2+}$. Emission spectrum obtained in DMSO/water at 77 K [89].

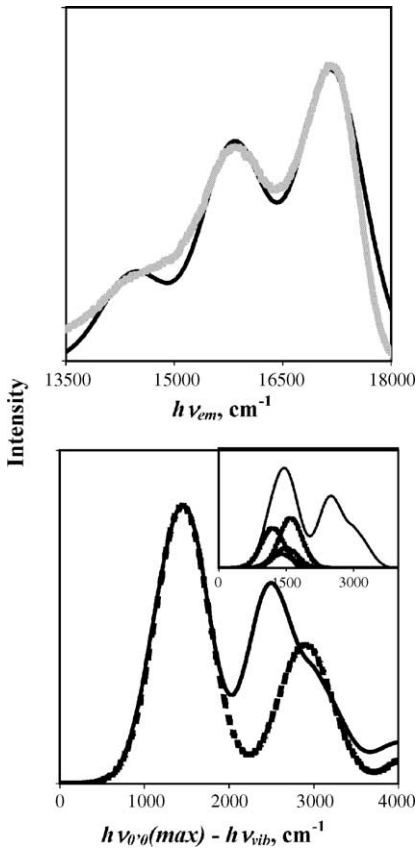

Fig. 7. Top: fit (black line) of $[Ru(bpy)_3]^{2+}$ emission (gray line) with a single high frequency vibronic component; five adjusted parameters (two peak heights, two peak energies, one bandwidth) with $\Delta\nu_{1/2} = 1050\,cm^{-1}$ (first and second order contributions only). Bottom: The envelope (or difference spectrum) of vibronic contributions constructed from the sum of four components (inset) with $\Delta\nu_{1/2} = 1000\,cm^{-1}$, solid line; an "equivalent", single vibronic component fit to the first order contribution of the vibronic envelope, dashed line. Second and third order contributions are included in both spectral constructions.

fit). This difference spectrum has distinct vibronic features centered at about 610, 1560 and 2710 cm^{-1}. The first of these is in the region of metal–ligand skeletal modes and metal–ligand torsional modes; the second is in the region of intraligand stretching modes. The relatively weak feature near 2700 cm^{-1} must be the result of higher order vibronic contributions from the vibrations between 1100 and 1360 cm^{-1} (see Eq. (32)). If one assumed that the 1360 cm^{-1} contribution resulted from a single vibrational mode, then the second order contribution of this mode to the intensity at 2720 cm^{-1} would be 0.405; the observed contribution is 0.339. This discrepancy is consistent with the 1360 cm^{-1} feature being the sum of several different vibronic contributions. It should be noted that the representation of the observed vibronic contributions by some single, "average frequency" distortion mode will necessarily require an inappropriately large bandwidth and it generally misrepresents the contributions of higher order vibronic contributions to the spectrum; these points are illustrated in Fig. 7. The fit of a single vibronic mode to the 77 K emission spectrum of $[Ru(bpy)_3]^{2+}$ can only be accomplished by choosing a value of $\Delta\nu_{1/2}$ that is approximately the average of the mean widths of the narrower high-energy peak and the broader low energy peak. This results in a very poor fit on the high-energy side of the emission spectrum. The second order vibronic contributions are also not well fit by a single vibronic mode model of $[Ru(bpy)_3]^{2+}$; this would be a major problem if one were trying to identify the vibronic contributions of higher energy vibrational modes, and the problem is more obvious if one removes the contribution of the fundamental from the spectrum. This is illustrated in the simple "difference" spectrum at the bottom of Fig. 7; this spectrum is constructed as the sum of four arbitrary "vibronic" components. The sum of these components can be reasonably well fitted by a single Gaussian peak, but the higher order components derived from this peak, based on Eqs. (32) and (33), grossly misrepresent the higher order vibronic components. The first and second order vibronic components are convoluted in the ambient emission

of the $[Ru(bpy)_3]^{2+}$ complex [89], and while the structureless emission can certainly be fit with a single vibronic component by adjusting the values of parameters in Eq. (21), the significance of the fitting parameters is not clear (see also comments in [58]).

3.2.5. *Vibronic contributions and their attenuation; evaluation in terms of empirical reorganizational energy profiles (emreps)*

The vibronic structure becomes more evident the lower the temperature. The 77 K emission spectra are emphasized in this section. In our search for the contributions of high frequency vibronic modes to the emission spectrum, we have evolved an approach that emphasizes the reorganizational energy contributions of those modes. This approach is based on the first order vibronic contributions, Eqs. (12) and (31). The emission spectrum is represented in Eqs. (30)–(35) as the sum over some sets of vibronic progressions (the components of a progression are designated by subscript *j*; different vibronic progressions by a subscript h) [53,54,58]. In order to evaluate the different vibronic contributions, the fundamental is subtracted from the emission spectrum (see above discussion) and the energy scale is defined by the energy difference from the fundamental (i.e., set $h\nu_{max}$(fundamental) = 0). In order to generate a graphical display that emphasizes contributions of the high frequency vibrational modes to the excited state distortion, the intensity and energy axes are rescaled.

a. The relative contributions to excited state distortion are emphasized when Eq. (12) is rearranged by solving for λ_h. The corresponding empirical profile of reorganizational energy contributions is generated by multiplying the difference between the observed emission intensity and the fundamental component intensity at each energy, $[I_{\nu_d(obsd)} - I_{\nu_d(f)}]$, by $h\nu_d/I_{max(f)} = [h\nu_{max(f)} - h\nu_m]/I_{max(f)}$. The vertical axis is then $h\nu_d[I_{\nu_d(obsd)} - I_{\nu_d(f)}]/I_{max(f)}$, where $I_{\nu_d(f)}$ is the intensity of the fundamental and $I_{\nu_d(obsd)}$ is the observed emission intensity at the frequency ν_d.
b. The rescaling of the energy axis is necessary because the vibronic components in the emission spectrum of these complexes have significant bandwidths (equal to that of the fundamental), and this, combined with the rescaling of the intensity axis results in the displacement of the maxima of the resulting profiles relative to the vibronic maxima of the difference spectra.

An approximate rescaling can be accomplished by the following procedure: The $0' \rightarrow 1$ transition of the *h*th displacement mode is represented by a Gaussian function of the form $I_{\nu_m(0'1)_h} = C\,e^{-x^2/a^2}$, where C is a constant independent of emission energy, $x = [\nu_{max(f)} - \nu_h - \nu_m]$ and $a = \Delta\nu_{1/2}/2(\ln 2)^{1/2}$. The maximum of the first band of the *h*th vibronic progression occurs at $\nu_m = [\nu_{max(f)} - \nu_h]$. The intensity rescaling is equivalent to replacing the Gaussian functions by functions of the type,

$$f = c \times \nu_d \times e^{-x^2/a^2} \tag{55}$$

The maximum of this function with respect to $\nu_d = (\nu_{max(f)} - \nu_m)$ is given by,

$$\frac{df}{d\nu_d} = C\,e^{-x^2/a^2}\left[\frac{1 + 2\nu_d\{\nu_h - \nu_d\}}{a^2}\right] = 0 \tag{56}$$

Thus, in this representation of the data, the maxima of f are observed at,

$$\nu_d = \tfrac{1}{2}\nu_h + \tfrac{1}{2}[\{\nu_h\}^2 + 2a^2]^{1/2} \tag{57}$$

This equation can be rearranged and solved for ν_h. The direct solution contains a correction term, a^2/ν_d, that is not useful for small values of ν_d, but an inverse Taylor's expansion leads to a frequency parameter that more generally corresponds to the frequencies of the displacement modes,

$$\nu_h = 2\nu_d - [\{\nu d\}^2 + a^2]^{1/2} \tag{58}$$

Note that $a = \Delta\nu_{1/2}/2(\ln 2)^{1/2}$ is simply a number for each spectrum; the value of $\Delta\nu_{1/2}$ is the full-width at half-maximum intensity obtained for the fundamental from the Gaussian fit of the emission spectrum.

A related correction must be made for the amplitudes of the reorganizational energy maxima. This can be approximately accomplished by substituting ν_x (calculated using Eq. (58), but noting the rescaled frequency by x rather than h) for ν_d. Thus, the final vertical axis is given by,

$$\Lambda_x = h\nu_x[I_{\nu_d(obsd)} - I_{\nu_d(f)}]/I_{max(f)} \tag{59}$$

Since the actual profile of reorganizational energies that is generated from the experimental emission spectrum is the envelope of the contributions of many different displacement modes, we have represented these empirical reorganizational energies and the corresponding vibrational energies with a subscript *x*.

The empirical reorganizational energy profiles (emreps) are generated by plotting λ_x versus $h\nu_x$. This use of Eqs. (58) and (59) in scaling the axes amounts to a first order iterative correction. Under some circumstances a higher order correction might be necessary. The correction terms are most important for small values of $h\nu_d$. The uncertainties are intrinsically large for very small values of $h\nu_d$ where the amplitudes of λ_x correspond to the differences between two large numbers, $I_{\nu_d(f)}$ and $I_{\nu_d(obsd)}$.

This presentation of the emission spectral data is illustrated for $[Ru(bpy)_3]^{2+}$ at the bottom of Fig. 6. Typically, the vibrational frequency of the maximum of the envelope of values of λ_x for these complexes is different from the maximum of the difference spectrum, although the reorganizational energies inferred from the maximum amplitudes are equivalent for the difference spectrum and the emrep. This difference in the vibrational frequencies associated with the respective maxima of these representations of the vibronic contributions

is consistent with the composite nature of the spectral envelope.

The amplitudes of the emreps have the dimensions of reorganizational energies, but they are composite values, not the reorganizational contributions of any specific mode. If their only contributions are from first order vibronic components, and if Eqs. (43) and (45) apply equally to all of the distortion modes, then changes in λ_x can be readily related to the effects of configurational mixing. It must be emphasized that this analysis is only useful when: (a) the contribution of the fundamental is independently and reliably determined; and (b) when the dominant contributions to λ_x arise from the first order vibronic components. The comparisons with resonance-Raman data indicate that these conditions are reasonably well met for the 77 K emission spectra of the $[Ru(NH_3)_{6-2n}(bpy)_n]^{2+}$ complexes. The determination of the reorganizational energies of specific vibronic components must depend on additional information (e.g., resonance-Raman spectra, the effects of isotopic substitution, etc.) for emission spectra with bandwidths as broad as observed in the CT emission spectra discussed here.

3.2.6. Vibronic contributions and their attenuation; correlation of reorganizational energies with excited state energy

The amplitudes of the difference spectra and the emreps give equivalent results (when the reorganizational amplitudes are evaluated), and either can be used in evaluating the attenuation effects associated with configurational mixing. We use the emreps for this purpose here to simplify the overall discussion since their amplitudes are expressed as reorganizational energies. Even at 77 K, the observed bandwidths are large enough that there are second order vibronic contributions to the observed emission spectra (and to the difference spectra and emreps that are generated from them) in the region 1300–1600 cm^{-1} lower in energy than $h\nu_{max(f)}$. Modellings of the emission spectra with the resonance-Raman data suggest that these contributions run in the range of 25–35% of the total vibronic contribution to the emreps of the Ru–bpy complexes in this region [89]. The attenuation of second order vibronic components is on the order of $(1 - 2\alpha^2_{RP} - 2\alpha^2_{PR})^2$, and appreciably stronger than that of the first order components (Eq. (45)); in principle; a quantitative interpretation of the observations described here should take this into account. In this article, the attenuation effects are presented in terms of correlations of empirical parameters, and some general implications are discussed. A more detailed analysis is being prepared [89].

The arguments outlined above indicate that the large values of the electronic matrix element, H_{RP}, for Ru–bpy complexes should lead to appreciable configurational mixing of the diabatic states, and that this configurational mixing should significantly alter the properties of the D/A complex. These effects should be most clearly manifested in the optical transition energies, bandwidths and vibronic structure

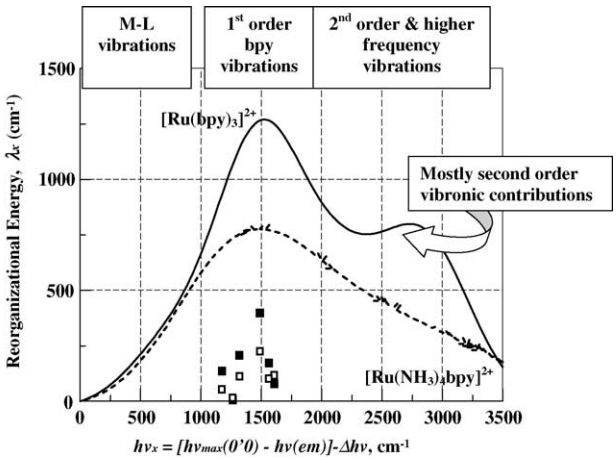

Fig. 8. Comparisons of reorganizational energy profiles for $[Ru(bpy)_3]^{2+}$ (upper, solid curve) and $[Ru(NH_3)_4bpy]^{2+}$ (lower, dashed curve) [89]. Points are resonance-Raman (r-R) data of Kincaid and co-workers (solid) [66] and of Hupp and co-workers (open) [65] for the respective complexes (see Table 2). The profiles indicate a reasonably consistent pattern of attenuation at 1500 cm^{-1} (note that contributions of Ru–ligand vibrations, higher order vibronic contributions and C-H and N-H vibrations are necessarily different). Some of the resonance-Raman data are less consistent; however, when the r-R intensities are represented as Gaussian functions with the bandwidth of the fundamental, the sum of their contributions approximates the respective normalized emission spectra and the emreps generated from these r-R-derived spectra are similar in amplitude to those obtained from experimental spectra.

in the D/A complexes. The reorganizational ($\lambda_{x(max)}$) and vibrational ($h\nu_{x(max)}$) parameters associated with the emrep maxima are summarized in Table 1. The emrep maxima occur at 1530 ± 30 cm^{-1} for the ammine–bpy complexes (Fig. 8 and Table 1), and at 1440 ± 30 cm^{-1} for en–bpy complexes (Table 1). The value of $\lambda_{x(max)}$ for $[Ru(NH_3)_4bpy]^{2+}$ is markedly smaller than that of $[Ru(bpy)_3]^{2+}$, see Figs. 8 and 9. The emission energy decreases in the same order, and configurational mixing will increase with the decreases of $h\nu_{max(f)}$. These observations are strong qualitative support for the predicted attenuation of reorganizational energy.

The vertical energies in the perturbation theory arguments refer to the diabatic energies; the observed emission energy maxima reflect the contributions of ground state stabilization due to configurational mixing, and the correction for this (in an estimate of the diabatic energies) has the opposite sign of the exchange energy contributions. We have based the correlations in Fig. 9 on Eqs. (43) and (45) and $E_{RP} \cong E_{PR} = h\nu_{max(f)}$. This assumes that the corrections for the exchange and stabilization energy contributions in estimates of the diabatic energies approximately cancel, and that H_{RP} is constant through the series of complexes. There is a small difference in the intercepts and slopes in DMSO/water and in butyronitrile; some of this is a consequence of the difference in bandwidths. However, the different solvents may also affect the excited state charge distribution and thereby the reorganizational energy associated with the bpy vibrational modes; this

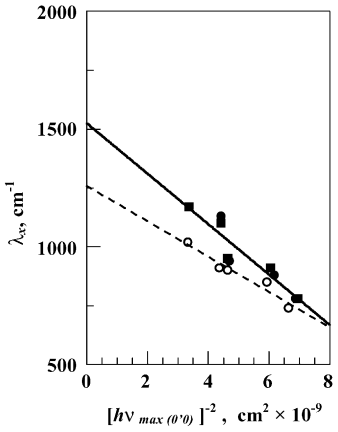

Fig. 9. Attenuation of reorganizational energies for $[Ru(Am)_{6-2n}(bpy)_n]^{2+}$ complexes in 77 K glasses [89]. Values of λ_x are from the emrep for each complex; values of $h\nu_{max(0'0)}$ are the maxima of the fundamental emission components based on Gaussian deconvolutions. DMSO/water (solid points): The least squares fit (black line) has a slope of (110 ± 20) × 10^{-3} cm and an intercept of (1500 ± 100) cm^{-1}. Black circles are for deutero-am(m)ine (ND) complexes. Butyronitrile (open circles): The least squares fit (dashed line) has a slope of (75 ± 10) × 10^{-3} cm and an intercept of (1260 ± 60) cm^{-1}.

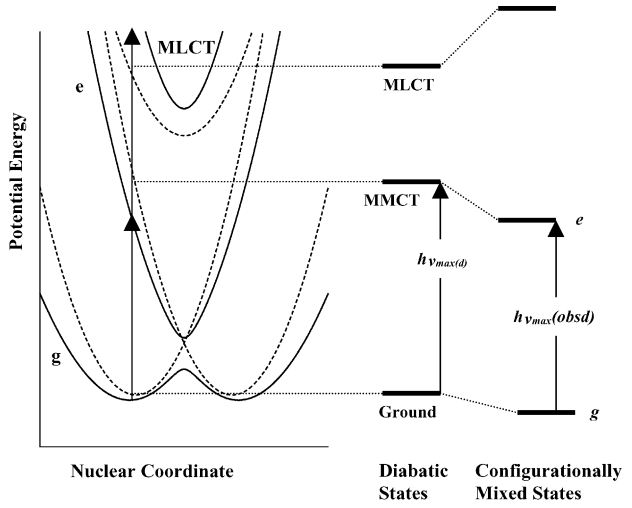

Fig. 10. Qualitative illustration of a covalently linked, degenerate donor/acceptor complex in which the electronic coupling is mediated by the bridging ligand. PE curves for diabatic states are shown as dotted lines, the PE curves for three configurationally mixed states are shown as solid lines.

possibility is currently being examined [89]. Overall, the correlation does demonstrate a strong attenuation of reorganizational energies through the series of complexes, qualitatively consistent with Eqs. (43) and (45), and the slopes of the correlation lines are reasonably consistent with the previous estimate H_{RP} for this family of complexes [60]. However, it is important to observe that the mixing coefficient implied for the $[Ru(NH_3)_4bpy]^{2+}$ complex is large enough that higher order terms probably contribute. A mixing coefficient for this complex of the magnitude implicated by Eq. (45) with $\alpha_{eg} < \alpha_{ge}$ corresponds to a large amount of electron density delocalized (≥25%) and a MLCT excited state that is far from the diabatic limit Fig. 10.

3.3. Summary

The studies considered in this section have dealt with some of the electron-transfer properties of Ru^{II}–bipyridine complexes in which the donor and acceptor are very strongly coupled. The relatively recent availability of near-infrared array detectors has enabled emission spectra to be collected for a wide range of relevant complexes. For strongly coupled systems in which electron-transfer ground and excited states are both lower in energy than the mediating donor/bridging ligand MLCT excited state (all energies with respect to the ground state nuclear coordinates), the results of these studies can be summarized:

a. The contributions of the high frequency vibrational modes to the 77 K emission spectra of $[Ru(NH_3)_{6-2n}(bpy)_n]^{2+}$ complexes are greatly attenuated as the energy of the fundamental component decreases. This marked attenuation of reorganizational energies can be attributed to the very strong D/A electronic coupling and the increases in configurational mixing that occur through this series of complexes. This appreciable attenuation of the reorganizational energy associated with the electron-transfer process can be interpreted in terms of variations in the fraction of electron density that is delocalized, α^2_{RP}. The apparent MLCT bandwidths may not decrease as predicted by the idealized arguments owing to the effects of the distribution of solvation environments and the convolution of other vibronic and/or electronic (in the case of absorption) bands into the spectral envelope; issues of optical resolution and difficulties in identifying the fundamental component (especially in ambient spectra) can also complicate the evaluation of the extent of reorganizational energy attenuation.
b. The observed emission spectra are for spin forbidden transitions of the lowest energy electronic excited states of these complexes. The trapping of the electronically excited complex in a spin state different from that of the ground state is attributable to a rate constant that is relatively small as a consequence of the small electronic matrix element.
c. Standard models [23,28–30,35,36,38,43,46,51,53,68,81] for the Marcus inverted region predict that large reorganizational energies, combined with small values of $E^{0'0}_{RP}$ and large electronic matrix elements result in rapid relaxation of the excited state. However, these models treat the three factors mentioned as independent variables, as in a weak-coupling limit. In this series of complexes these three factors are not independent of one another and the description of the reaction coordinate is very complicated.

4. The effects of bridging ligands on the properties of an electron-transfer system when there is appreciable metal/bridging ligand configurational mixing

4.1. General description and perturbation theory-based expectations

The systematic discussion of such linked donor/acceptor systems requires consideration of at least three electronic states: the two electron-transfer states, which are not directly mixed, and a metal/bridging ligand state (e.g., a MLCT excited state) that mixes them [3,7,16,18,19,21,23,42,78,98]. This approach is illustrated in Fig. 10.

At least in principle, the use of a three (or more) state limit for bridged D/A systems preserves the experimentally approachable diabatic reference mentioned above; the use of a two state model to describe such systems generally requires a different definition of the diabatic limit. The electronic configurations of the diabatic states are: (a) electron in a donor orbital (electron-transfer ground state); (b) electron on the acceptor orbital (electron-transfer excited state); (c) electron on the bridging ligand (metal to ligand charge transfer, MLCT, excited state). In the limit that $H^0_{RP} = 0$ (no direct donor/acceptor orbital overlap) the corresponding wavefunctions are,

$$\psi_R = \frac{\psi_{R(d)} + \alpha_{RB}\psi_{B(d)}}{[1+\alpha^2_{RB}]^{1/2}} \tag{60}$$

$$\psi_P = \frac{\psi_{P(d)} + \alpha_{BP}\psi_{B(d)}}{[1+\alpha^2_{BP}]^{1/2}} \tag{61}$$

$$\psi_B = \frac{\psi_{B(d)} - \alpha_{RB}\psi_{R(d)} - \alpha_{BP}\psi_{P(d)}}{[1+\alpha^2_{RB}+\alpha^2_{BP}]^{1/2}} \tag{62}$$

Since the energies are evaluated with respect to a single set of nuclear coordinates (those of one of the PE minima), $\alpha_{RB} = \alpha_{BR}$ and $\alpha_{PB} = \alpha_{BP}$ in Eqs. (60)–(62).

Most of the studies of linked transition metal D/A complexes have employed bridging ligands that have relatively low energy π-type LUMOs and metals in which the electron-transfer process involves dπ-orbitals [16,19]. There are fewer studies of purely σ analogs. Some general features of the perturbation theory arguments apply to any type of bridging ligand.

Electron-transfer mediated by configurational mixing with a bridging ligand MLCT excited state is typical of the majority of linked transition metal D/A systems. The electron-transfer can also be mediated by a ligand to metal charge transfer (LMCT) bridging ligand state, $\{(D) - (B^+) - (A^-)\}$. These are commonly referred to as the "electron" and "hole" transfer mechanisms, respectively. The electron-transfer mechanistic formulation is the focus of this article. For H_{DB}/E_{DB} and H_{BA}/E_{BA} the coefficients for mixing donor and acceptor orbital wavefunctions with a single bridging ligand orbital wavefunction (assuming that the three state model can be represented in terms of three orbitals, with a partly filled acceptor orbital and a filled donor orbital, as in a d^6_p/d^5_p complex, and a vacant bridging ligand orbital, as in a π^*-orbital) [18,22],

$$H^{spx}_{DA} = \frac{H_{DB}H_{BA}}{2E_{av}} \tag{63}$$

The energy parameter in the denominator of Eq. (63) is based on vertical energies, usually obtained from the charge transfer spectra of the metal complexes [22],

$$E_{av} = \frac{2E_{DB}E_{A^-B}}{(E_{DB}+E_{A^-B})} \tag{64}$$

If the bridging ligand is composed of a chain of weakly coupled units ($B^{(1)}$, $B^{(2)}$, …, $B^{(n)}$), and when only the interactions between nearest neighbor moieties of the bridging ligand are considered (γ_{ij} = the mixing coefficient between the ith and jth bridging ligand moieties) the D/A coupling matrix element can be generalized as [22,23,98,99],

$$H^{spx}_{DA} = \frac{H_{DB^{(1)}}}{E_{DB^{(1)}}}\left[\prod_{(i)=1}^{(i)=n-1}\gamma_{(i)(i+1)}\right]H_{B^{(n)}A} \tag{65}$$

In the limit of an infinite chain of identical bridging ligand moieties, Eq. (65) takes the form of an exponential dependence on the geometrical distance between the donor and acceptor, d_{DA} [22,23,98,99],

$$H^{spx}_{DA} = H_{DA}(i=0)\,e^{-\beta d_{DA}} \tag{66}$$

An algebraically similar expression can be based on the overlap of spherical wavefunctions far from their nuclei of origin [100], and in this case β is an inverse orbital radius.

Configurational mixing of the donor (ground state) and acceptor (excited state) with the ligand electronic states reduces the energies of the electron-transfer ground and excited states by $\varepsilon_s(R) = H^2_{DB}/E_{DB}$ and $\varepsilon_s(P) = H^2_{AB}/E_{AB}$, respectively. As a consequence, configurational mixing with the MLCT excited state of the bridging ligand shifts the absorption maximum of the $D \rightarrow A$ electronic transition to lower energy since $E_{DB} > E_{AB}$ (with respect to the ground state nuclear coordinates; see Fig. 11),

$$\begin{aligned} h\nu_{max}(D/A) &= h\nu_{max}(\text{ref}) + \varepsilon_s(R) - \varepsilon_s(P) \\ &= h\nu_{max}(\text{ref}) + \alpha^2_{RB}E_{RB} - \alpha^2_{PB}E_{PB} \end{aligned} \tag{67}$$

The reference chosen for evaluating this shift is a D/A complex in which there is no configurational mixing ($H_{DB} = H_{AB} = 0$) and for the same general conditions as in the system investigated. The shifts in the absorption maxima are measures of the configurational mixing with the bridging ligand in strongly coupled systems. For a chemically symmetric system, $H_{RB} = H_{PB}$, and when no other factors contribute to

the shifts in absorption maximum,

$$\Delta h\nu_{max} = \left[h\nu_{max}(\text{ref}) - h\nu_{max}(D/A)\right] = H_{RB}^2\left(\frac{E_{RB} - E_{PB}}{E_{RB}E_{PB}}\right) \quad (68)$$

Eqs. (63) and (67) can be combined for a simple, chemically symmetrical system, (assuming one partly filled acceptor orbital, as in Ru^{II}/Ru^{III} couples) to relate the shift of the absorption maximum to the single, linker MLCT excited state mediated superexchange coupling [101,102].

$$\Delta h\nu_{max} \cong 4\,H_{DA}^{spx}\left[\frac{E_{DA}}{E_{DB} + E_{AB}}\right] \quad (69)$$

Appropriate parameters can often be inferred from the properties of related, but separate donor and acceptor complexes, or from the extrapolation the properties of a series of closely related complexes to the limit in which $H_{DA} = 0$.

4.1.1. Illustrations of the three state limit: complexes based on Taube's work with aromatic bridging ligands

There have been a very large number of studies of $d\pi^6/d\pi^5$ metals (Fe^{II}/Fe^{III}, Ru^{II}/Ru^{III}, Os^{II}/Os^{III}, Re^{I}/Re^{II}, etc.) with $p\pi$ bridging ligands (pyrazine, polypyridines, N_2, CN^-, etc.) [3,16,18–20,25]. Only selected parts of this work will be considered here.

A large number of complexes have been prepared in which the donor and acceptor are bridged by 4,4′-bipyridine, pyrazine and closely related ligands [3,10,11,16,18–20,103,104]. The metal–ligand electronic coupling is very strong in all of these complexes based either on their electronic absorption spectra (typical MLCT absorptivities at maximum are $\geq 3000\,M^{-1}\,cm^{-1}$) [18] or electroabsorption spectra (H_{RP} between 4000 and 11,000 cm^{-1}) [73,87,105,106]. The bb-bridged complexes discussed in Section 2.6 above demonstrate that very strong metal–ligand electronic coupling ($H_{RuL} \approx 7 \times 10^3\,cm^{-1}$ [60,62,63]) does not necessarily imply strong ligand-mediated metal–metal coupling ($H_{MM'} \ll 10^2\,cm^{-1}$ for the bb-bridged complexes [78,79]).

Appreciably stronger metal–metal coupling is mediated by 4,4′-bipyridine and related ligands [10,11,16]. The values for H_{DA} estimated for these complexes are within the range of values found for ion pairs, but much larger than found for the bb-bridged complexes [21]. Nevertheless, the fraction of delocalized electron density, α_{RP}^2, is small, and the configurational mixing (or electronic coupling) in most of these complexes can be considered to be relatively weak. In order to estimate the value of $h\nu_{max}$ in the limit that $\alpha_{IB}^2 \to 0$, one can combine Eq. (29) with Eqs. (67)–(69) to describe the variations of $h\nu_{max}$ of a closely related series of complexes in which the configurational mixing varies. The energies of the intervalence absorption maxima, $h\nu_{max}$(MMCT), for complexes of the type $[\{Ru(NH_3)_5\}_2B]^{5+}$ (where B is a di-pyridyl bridging ligand [10,11,16]) do decrease systematically as the absorptivity of the MMCT transition increases (Fig. 11), in qualitative accord with expectation based on Eq. (69). This correlation neglects systematic deviations that occur as $4\alpha_{RP}^2$ becomes significant compared to unity and the relatively small variations in MLCT energies through the series of complexes.

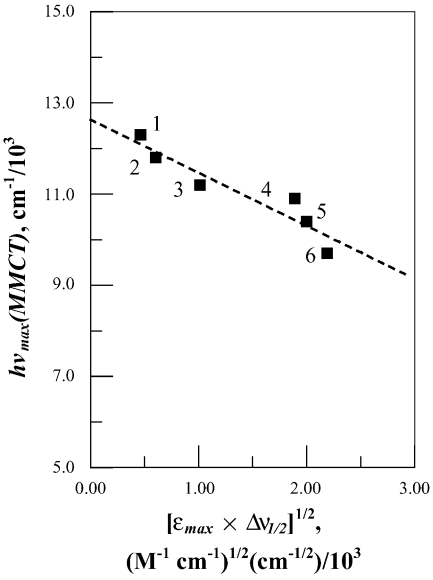

Fig. 11. Correlation of decreases in transition energy with increases the absorptivity of the Ru^{II}/Ru^{III} MMCT absorption (Data of Sutton and Taube [10,11]) for $[\{Ru(NH_3)_5\}_2L]^{5+}$ complexes. L = *bis*-(4-pyridyl)methane, **1**; 3,3′-bipyridine, **2**; 3,3′-dimethyl-4,4′-bipyridine, **3**; 1,2-*bis*-(4-pyridyl)acetylene, **4**; *trans-bis*-(4-pyridyl)ethylene, **5**; 4,4′-bipyridine.

Extrapolation of the plot of $h\nu_{max}$(MMCT) versus $(\varepsilon_{max}\Delta\nu_{1/2})^{1/2}$ to zero absorptivity indicates that $h\nu_{max}$(ref) $\cong (12.6 \pm 0.3) \times 10^3\,cm^{-1}$. This is very similar to the value of $\chi_r = 12.1 \times 10^3\,cm^{-1}$ estimated for the $[Ru(NH_3)_5py]^{3+,2+}$ couple [21]. The value of $h\nu_{max}$(ref) $\cong 12.6 \times 10^3\,cm^{-1}$ leads to $\Delta h\nu_{max}$(obsd) $\cong 2.9 \times 10^3\,cm^{-1}$ for $[\{Ru(NH_3)_5\}_2(4,4'\text{-bpy})]^{5+}$. Electroabsorption measurements have been used to determine that $H_{DB} = 5.5 \times 10^3\,cm^{-1}$ for $[Ru(NH_3)_5(4,4'\text{-bpy})]^{2+}$ [87]. This and the other spectroscopic parameters combined with Eq. (69) imply that $\Delta h\nu_{max}$(calcd) $\approx 3.4 \times 10^3\,cm^{-1}$; this is good consistency given that there is probably a systematic error in the extrapolation of Fig. 11 due to neglect of variations in the MLCT energies and higher order perturbational terms. These parameters and Eq. (69) suggest that $H_{DA}^{spx} = 1.6 \times 10^3\,cm^{-1}$. However, electroabsorption measurements indicate that H_{DA}^{spx} is actually about $750\,cm^{-1}$ [105,106]. This difference may arise from treating 4,4′ bpy as a single bridging moiety. If it is treated as a combination of two linked pyridines, then Eq. (65) and the electroabsorption measurements imply that $\gamma_{py,py} \approx 0.4$. These di-pyridyl-linked complexes illustrate the features expected based on Fig. 2 and Eqs. (65) and (67)–(69); superexchange coupling in a closely related series of bridged complexes

correlates inversely with the energy of the donor/acceptor electronic transition and directly with the absorptivity of that transition.

4.2. Entanglement of the nuclear and electronic coordinates: vibronic coupling in CN-bridged complexes

The complexes in which cyanide bridges a transition metal donor complex to a transition metal acceptor complex have exhibited a remarkable array of properties that do not fit neatly into all of the approaches outlined above.

4.2.1. The variations of the C≡N stretch with the oscillator strengths of MM′CT transitions in cyanide-bridged D/A complexes

The CN-stretching frequencies of cyanide-bridged M(CN)M′ complexes tend to be shifted to low energy when M and M′ form a strongly coupled D/A pair [102,107,108]; Fig. 12 graphically presents some representative observations. Two cyanide stretches are observed in the IR spectra of dicyano complexes such as *trans*-[([14]aneN$_4$)Cr(CNRu(NH$_3$)$_5$)$_2$]$^{5+}$ and the *trans*-[([14]aneN$_4$)Cr(CN)$_2$]$^+$ parent [107–109]. The symmetric combination of stretches shifts from 2137 cm^{-1} in the parent to 1996 cm^{-1} in the *trans*-[([14]aneN$_4$)Cr^{III}(CNRu^{II}(NH$_3$)$_5$)$_2$]$^{5+}$ complex; the antisymmetric combination shifts only from 2096 cm^{-1} to 2077 cm^{-1}, respectively. Fig. 13 presents the shifts of ν_{CN} in more detail for *trans*-[(*ms*-Me$_6$[14]aneN$_4$)Cr(CNRu(NH$_3$)$_5$)$_2$]$^{5+}$, *cis*-[(*rac*-Me$_6$[14]aneN$_4$)Cr(CNRu(NH$_3$)$_5$)$_2$]$^{5+}$, their parent dicyano complexes and the rhodium(III)-centered analogs. The shifts observed for *cis*-[(*rac*-Me$_6$[14]aneN$_4$)Rh(CNRu(NH$_3$)$_5$)$_2$]$^{5+}$, relative to ν_{CN} for the parent, are to slightly higher energy and qualitatively in the direction expected for the kinematic (or mechanical) coupling of C-N, M-C and N-M′ oscillators [110]. The observed values of ν_{CN} are shifted strongly in the opposite direction upon ruthenation of the Cr^{III}-centered complexes. The symmetric combination of cyanide stretching frequencies in *trans*-[(*ms*-Me$_6$[14]aneN$_4$)Cr(CNRu(NH$_3$)$_5$)$_2$]$^{5+}$ is shifted by the greatest amount, but the shift is equally distributed in the CN-stretches of *cis*-[(*rac*-Me$_6$[14]aneN$_4$)Cr(CNRu(NH$_3$)$_5$)$_2$]$^{5+}$ (the CN stretches were identified by the shifts when the complexes were prepared with ^{13}CN$^-$; the band identified as the antisymmetric combination of CN stretches in the *trans*-complexes was 4–10 times more intense than the symmetric combination [108]). The magnitude of this shift to lower energies, $\Delta\nu_{CN}$, has been found to increase with the oscillator strength of the donor/acceptor charge transfer (MM′CT) absorption [107,108]. The absorptivity of the Ru^{II}/Cr^{III} MM′CT band (λ_{max} = 500 nm) is 7600 M^{-1} cm^{-1} in this complex. The analogous Rh^{III}-centered complex (λ_{max} = 342 nm, ε_{max} = 800 M^{-1} cm^{-1} for the MM′CT transition) exhibits much smaller shifts of ν_{CN} (2142–2156 and 2124–2114 cm^{-1}, respectively). Since the effect is mostly in the symmetric *combination* of stretches, the effect is in one molecular

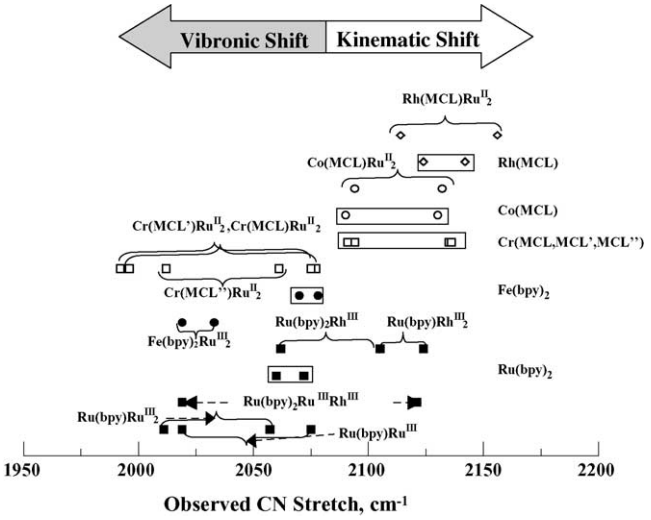

Fig. 12. Shifts of the CN stretching frequency that accompany metallation of coordinated cyanide in [M(L)(CN)$_n$M′]$^{m+}$ complexes. The parent dicyano and cyano complexes are listed on the right and their CN stretching frequencies are enclosed in rectangular boxes. These complexes are formally M^{III} for the M^{III}(MCL) complexes and M^{II} for the M(bpy)$_2$ complexes. For the Cr^{III} complexes, MCL = [14]aneN$_4$, MCL′ = *ms*-Me$_6$[14]aneN$_4$ and MCL″ = [15]aneN$_4$; for the Co^{III} and Rh^{III} complexes, MCL = [14]aneN$_4$. Ru^{III} designates Ru(NH$_3$)$_5^{3+}$ and Rh^{III} designates Rh(NH$_3$)$_5^{3+}$ for the M(bpy)$_2$ complexes; for the M^{III}(MCL) centered complexes, Ru^{II} designates Ru(NH$_3$)$_5^{2+}$. The block arrows at the top indicate the sense of the kinematic shift that is expected to occur upon metallation of coordinated cyanide and the vibronic shift that is observed when CN bridges a strongly coupled donor and acceptor. The frequencies are from [108,109].

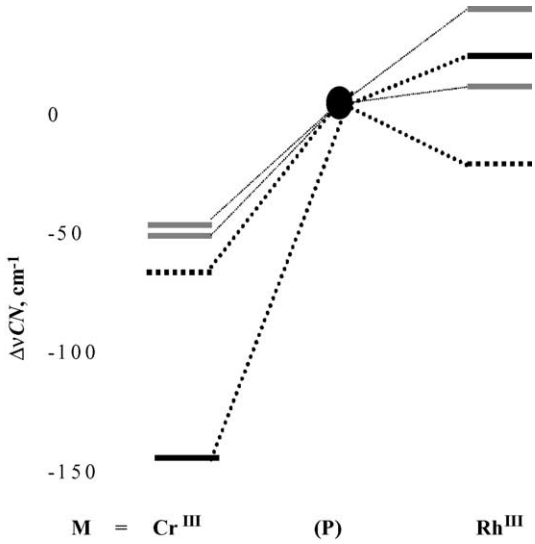

Fig. 13. Shifts of the CN stretch, $\Delta\nu_{CN}$ = [$\Delta\nu_{CN}$(ruthenate) − $\Delta\nu_{CN}$(parent)], for *trans*-[M^{III}(*ms*-Me$_6$[14]aneN$_4$)(CNRu^{II}(NH$_3$)$_5$)$_2$]$^{2+}$, dark lines, and *cis*-[M^{III}(*rac*-Me$_6$[14]aneN$_4$)(CNRu^{II}(NH$_3$)$_5$)$_2$]$^{2+}$, grey lines. For the *trans*-complexes, the symmetric combination oc CN stretches is designated by the solid line and the antisymmetric combination by the dashed line. The frequencies of the CN stretches in the parent [M^{III}(MCL)(CN)$_2$]$^+$ complexes, (P), are represented at the origin by the solid ellipse. Data from [108,109].

normal vibrational mode of the *trans*-complexes, equally distributed over the two bridging cyanides and not localized in either.

Overall, for several complexes of different symmetries, the magnitude of $\Delta\nu_{CN}$ (referenced in each case to the analogous Rh^{III} complex) is proportional to the oscillator strength of the MM′CT transition [102]. This implies a correlation of the changes in one of the nuclear coordinates (the C≡N stretch or Q_{CN}) with changes in the electronic coupling between the donor and acceptor.

4.2.2. Vibronic models to account for the decreases of ν_{CN} with increases of MM′CT oscillator strength

A simple vibronic model for describing these systems (analogous to pseudo-Jahn-Teller models [111,112]) assumes that: (a) the delocalization of electron density from the donor onto the bridging ligand, and/or from the bridging ligand onto the acceptor weakens the C≡N bonds; and (b) a weakened C≡N bond results in enhanced D and A coupling to the bridging ligand [107,109]. This model has been demonstrated to be consistent with the proportionality between the shifts of ν_{CN} and the MM′CT oscillator strength [107,108,113,114]. The principal assumption of this model can be represented as [107,109,113,114],

$$H_{RP} = H^0_{RP} + bQ_{CN} \tag{70}$$

The H^0_{RP} term allows for any direct Ru^{II}/Cr^{III} electronic coupling (i.e., not mediated by the bridging cyanide). Eq. (70) contrasts to the common assumption that H_{RP} is independent of the nuclear coordinates (Condon approximation) [22,42]. It also contrasts to normal superexchange coupling models. Configurational mixing in the three state model results in modification of the ground (g) and excited state (e) potential energy functions so that $PE_J \cong (PE^{0'0}_k + kQ^2_N/2 - \varepsilon_{JL})$, where $PE^{0'0}_j$ is the difference in energy between the unmixed (diabatic), vibrationally equilibrated electron-transfer states (PE minima at $Q_N = 0$ and Q^0_N, respectively, where the superscript "0" designates a quantity defined with respect to the diabatic PES') and J = g or e. In the "vibronic" model the $\varepsilon_{JL} = (H^0_{RP} + bQ_{CN})^2/E^0_{RP})$ are expanded in a Taylor's series around the relevant nuclear coordinates to obtain Eq. (71) [107,109,113,114],

$$PE_g \cong kQ^2_N/2 - \varepsilon^0_{DL} - aQ_N \tag{71a}$$

$$PE_e \cong PE^{0'0}_P + 1/2\,k(Q^0_N - QN)^2 - \varepsilon^0_{AL} + a'Q_N \tag{71b}$$

where k is a force constant and a, a' and b are linear vibronic coefficients from the Taylor's expansions. This argument results in a functional relationship between $\Delta\nu_{CN}$ and the MM′CT oscillator strength that is qualitatively consistent with observations [107–109,113,114]. An intuitively appealing variation on this model involves the two electron-transfer states coupled by means of mixing with D/CN^- MLCT and CN^-/A LMCT excited states. This would allow for a shift of electron density across the molecule in the ground state to achieve an interaction somewhat analogous to that proposed for D/A complexes with acetylenic bridges [115,116].

4.2.3. The di-cyano complexes as bridging ligands in mixed valence complexes: a vibronic selection rule

The dicyano complexes such as *trans*-[([14]aneN$_4$)$Cr(CN)_2]^+$ can function as bridging ligands between a donor and an acceptor. The separation of the terminal metals in the resulting hetero-trimetallic complexes, such as *trans*-[([14]aneN$_4$)Cr(CN $Ru(NH_3)_5)_2]^{6+}$, is about 10.5 Å, or very similar to that in complexes bridged by 4,4′-bipyridine. The lowest energy CT excited state that might configurationally mix with the ground state of *trans*-[([14]aneN$_4$)Cr(CN $Ru(NH_3)_5)_2]^{5+\text{ or }6+}$ is the $Ru^{II} \rightarrow Cr^{III}$ MLCT excited state. The $Ru(NH_3)_5{}^{3+,2+}$ half-wave potentials vary with the $Ru^{II} \rightarrow$ (central metal) MM′CT energies and absorptivities in the general manner expected for two state configurational mixing [109,113,114] for complexes of the types $[\{Ru(NH_3)_5\}_n(Am)_{6-n}M(CN)_n]^{(3+n)+}$ (M = Cr^{III}, Co^{III}, or Rh^{III}) and $[M(PP)_2(CNRu(NH_3)_5)_n(CN)_2]^{(3n\text{ or }[2n+1])+}$ (PP = bpy or 1,10-phenanthroline; M = Ru^{II}, Fe^{II} or M = Cr^{III}, Co^{III}, or Rh^{III}). This configurational mixing ($\{Ru^{II}(NH_3)_5/M^{III}(MCL)\}$ with $\{Ru^{III}(NH_3)_5/M^{II}(MCL)\}$) correlates with the shifts in $h\nu_{max}$ for the (terminal $\rightarrow$ terminal) $Ru^{II} \rightarrow Ru^{III}$ MMCT transition in the $[(MCL)M(CNRu(NH_3)_5)_2]^{6+}$ complexes (MCL = a tetraaza-macrocyclic ligand and M = Cr^{III}, Co^{III}, or Rh^{III}). However, this MM″CT transition has an absorptivity of ε_{max} = $120 \pm 40\,M^{-1}\,cm^{-1}$ nearly independent of M and the $Ru^{II} \rightarrow$ (central metal) MM′CT energy and absorptivity [101]. Thus, the $Ru^{II} \rightarrow$ (central metal) configurational mixing does not contribute in the manner expected for superexchange coupling (Eq. (69)). Fig. 14 illustrates the contrast in the superexchange coupling contributions of the substituted-dipyridyl complexes of the Sutton and Taube work (Fig. 12) to that of the dicyano-complex-bridged systems. It appears that the superexchange coupling pathway has been quenched in the $\{Ru(NH_3)_5\}_2(MCL)M(CN)_2]^{6+}$ complexes. This can be attributed to the cyanide-mediated, vibronic coupling (described above) by means of the simple model described below.

The D/A coupling can be very complicated in complexes with more than one *vibronically* coupled D/A pair [117,118]. In order to account for the failure of superexchange-like behavior in the dicyanocomplex-bridged systems, we have proposed a simple extension of the bimetallic vibronic model (sketched above) for trimetallic, M(NC)M′(CN)M″ systems [101,108]: (1) the CN^--mediated, M/M′ and M′/M″ coupling is treated as a "local", D(NC)A(CN)A′, interaction (D = donor; A, A′ = acceptors) as above; (2) the overall effect on ν_{CN}, in D(NC)A(CN)D systems [108], or on M/M″ coupling, in D(NC)A(CN)A′ systems is treated in terms of the perturbational mixing of these local interactions. The assumption that $H_{RP} \cong H^0_{RP} + bQ_{CN}$ implies that the ground state nuclear coordinates of the bridging CN^- are configured for strong(s)

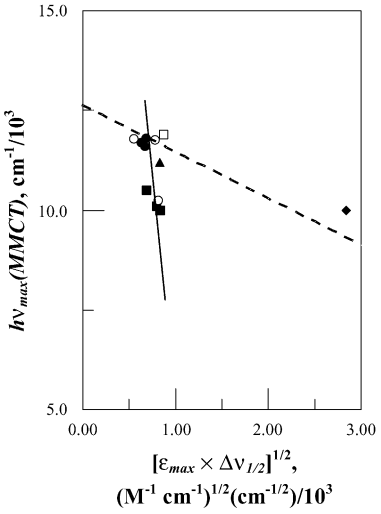

Fig. 14. Correlation of decreases in transition energy with increases the absorptivity of the Ru^{II}/Ru^{III} MMCT absorption (Data of Sutton and Taube, Fig. 11 for $[\{Ru(NH_3)_5\}_2M(L)(CN)_2]^{n+}$ complexes (data of Macatangay et al. [101,102]). The dashed line is the correlation line from Fig. 11. Closed symbols for *trans* complexes; open symbols for *cis* complexes. Squares for Cr^{III}(MCL) complexes; circles for Rh^{III}(MCL) complexes; triangle for $Co^{III}(Me_6[14]aneN_4)$ complex; diamond (right hand side) for $Ru^{II}(py)_4$ complex. The MLCT energies of the dicyano-metallate- and the dipyridyl-bridged complexes are comparable, H^2_{DL} is about four times larger in the latter, so a more shallow slope is expected to the cyano-bridged than for the pyridyl-bridged complexes. See Eqs. (63), (64), (67) and (68)).

D/A coupling ($bQ_{CN} \gg H^0_{RP}$) in the $D(CN)_sA'$ moiety and for weak (or "kinematic" [110]; *w*) coupling ($bQ_{CN} \approx 0$) in the $A'(CN)_wA''$ moiety. The optical MM″CT transition leaves these coordinates fixed on generating an electron-transfer excited state,

$$[Ru^{II}(NC)_sM^{III}(CN)_wRu^{III}]g + h\nu \rightarrow {}^*[Ru^{III}(NC)_sM^{III}(CN)_wRu^{II}]_e \quad (72)$$

According to the vibronic model, the Ru^{II}/M^{III} electronic coupling (H_{EL}) should be small in the Franck-Condon excited state. The CN^- nuclear coordinates are expected to be between the s and w extremes in the vibrationally equilibriated MLCT excited state, $[Ru^{III}(NC)_iM^{II}(CN)_iRu^{III}]_L$, and the CN^- nuclear coordinates of the two vibrationally equilibriated electron-transfer states correspond to extrema of the anti-symmetric combination of CN^- stretches in the MLCT excited state (L). In view of this and the symmetry of the electron-transfer system, H_{DL} and H_{AL} are expected to be complementary, or out of phase functions of the CN^- nuclear coordinates. Several functions can be used to express this; among the simpler ones for the local, cyanide-mediated coupling with the central metal are,

$$H_{DL} \cong (H^0_{DL} + bQ^0_{CN} \cos\theta) \quad (73)$$

and

$$H_{AL} \cong (H^0_{AL} + bQ^0_{CN} \sin\theta) \quad (74)$$

for $0 \le \theta \le \pi/2$. To make the illustrative argument simpler, assume that $H^0_{DL} \cong H^0_{AL} \cong 0$ in the superexchange contribution. Then Eq. (63) becomes,

$$H^{spx}_{DA} = \frac{H_{DL}H_{AL}}{2E_{av}} = \frac{(bQ^0_{CN}\cos\theta)(bQ^0_{CN}\sin\theta)}{2E_{av}} \quad (75)$$

For the ground state coupling maximized between Ru^{II} and Cr^{III}, $\cos\theta = 1$ and $\sin\theta = 0$; thus, when evaluated in the ground state nuclear coordinates, $H^{spx}_{DA} = 0$. This is consistent with the observations on most of the dicyanocomplex-bridged D/A complexes [101]. The specific functions employed (i.e., $\cos\theta$ and $\sin\theta$) illustrate the general features of the model, but are not derived from it. In any event this simple "vibronic" model does suggest that there are conditions for which the matrix elements can approach zero, and amounts to a "selection rule" for H^{spx}_{DA} and for electronic coupling in a linked donor/acceptor complex.

The general features of this discussion of the electron-transfer spectroscopy in the cyanide-bridged complexes have been formulated in terms of a three state model such as illustrated in Fig. 10. In order for this approach to be applicable, the three configurationally mixed electronic states, the ground and excited electron-transfer states and the MLCT excited state (here designated g, e and L), must be sufficiently separated in energy, that their properties are not greatly altered by the configurational mixing between them (e.g., see Fig. 10; all energies evaluated with respect to the ground state nuclear coordinates); i.e., $\alpha^2_{JL} < 0.25$ (J = g, e). When the MM″CT and the MLCT excited states are approximately degenerate (i.e., for $H_{eL} \ge E_{eL}$), and when $H_{eL} > 0$, these electronic excited states will be thoroughly mixed,

$$\psi_+ = [\psi_{e(d)} + \psi_{L(d)}](2)^{-1/2} \quad (76)$$

$$\psi_- = [\psi_{L(d)} - \psi_{e(d)}](2)^{-1/2} \quad (77)$$

The energy difference between the mixed states will be approximately $2H_{eL}$, but this matrix element does not enter into the expressions for either of their wavefunctions. The superexchange matrix element in a cyanide-bridged complex for which this is the case takes the form,

$$H^{spx}_{DA} \cong \tfrac{1}{\sqrt{2}}\langle\psi_{g(d)}|H|\psi_+\rangle \approx H_{DL} \quad (78)$$

Thus, the degeneracy of the two diabatic excited states removes the constraint on superexchange coupling in the vibronically coupled system. In this limit of course, the electron in the excited state is delocalized over the acceptor (M″) and the bridging ligand (in this case the metal-di-cyanide moiety), so the distinctions between the metal and ligand localized states is lost and the charge transfer transitions should no longer be described as MM″CT and MLCT [84].

Arguments presented in the preceding sections (e.g., the extrapolation in Fig. 12) indicated that the diabatic energy for the $Ru(NH_3)_5^{3+,2+}$ couple in a bridged complex is approximately (12–13) $\times$ $10^3\,cm^{-1}$. The diabatic energies for the MM′CT transitions of the complexes that

are employed to approach this limit can be based on Eq. (22) and information available in the literature [2,21,70]. The available information indicates that the most likely candidates are dicyano-ruthenium complexes with values of $E_{1/2}(Ru^{III}/Ru^{II})$ smaller than that of $[Ru(bpy)_2(CN)_2]$ ($E_{1/2} \sim 0.9$ V). The *trans*-$[Ru(py)_4(CN)_2]$ complex [119] ($E_{1/2} = 0.74$ V [102,119]) has approximately the necessary properties. The $Ru^{II}(py)_4(CN)_2 \rightarrow Ru^{III}(NH_3)_5{}^{3+}$ transition in the *trans*-$[\{Ru^{III}(NH_3)_5\}_n\{Ru^{II}(py)_4(CN)_2\}]^{3n+}$ complexes ($n = 1, 2$) occurs at $(13.4–14.6) \times 10^3\ cm^{-1}$ with absorptivities of $2100–2700\ M^{-1}\ cm^{-1}/Ru^{III}$. The *trans*-$[\{Ru^{II}(py)_4(CNRu(NH_3)_5)_2\}]^{5+}$ complex easily satisfies the condition of $\alpha^2_{eL} > 0.25$ for extensive excited state mixing. This complex exhibits two low energy CT transitions (at 10,000 and 14,300 cm^{-1}), both with absorptivities of about $1500\ M^{-1}\ cm^{-1}$. The lower energy absorption band is at least 10 times greater than the absorptivity of the MM′′CT transition of the chromium-centered analog discussed above, indicating much greater electronic coupling with the electron-transfer excited state (despite the fact that the MLCT (or MM′CT) transition is 30% smaller in the ruthenium-centered than in the chromium-centered complex), and the higher energy band has a smaller absorptivity than the central-to-terminal transition of the *trans*-$[\{Ru^{II}(py)_4(CNRu(NH_3)_5)_2\}]^{6+}$ complex, consistent with "intensity stealing" by the lower energy transition. This comparison is a strong confirmation of the vibronic coupling arguments presented above.

4.3. Polypyridine bridging ligands

4.3.1. Some aspects of the molecular orbital structure of polypyridine ligands

Some features of aromatic bridging ligands are usefully discussed with respect to the 4,4′-bipyridine bridging ligand. Simple perturbation theory logic suggests that the properties of the of 4,4′-bipyridine linker can be regarded as a combination of the slightly modified properties (represented by ψ_{py}) of the two pyridyl moieties,

$$\psi_{bpy\pm} = \frac{\psi_{py} \pm \alpha_{py,py'}\psi_{py'}}{(1 + \alpha^2_{py,py'})^{1/2}} \quad (79)$$

The simplest limit arises when the effectiveness of the bridging ligand in mediating the electronic coupling of the donor and acceptor is only a function of the MLCT states that involve the LUMO of the bridging ligand; see Section 4.1 above. In this limit, Eq. (79) implies a four state model (MLCT excited states involving the two different pyridyl moieties; see also Eq. (65)), but the approach is otherwise similar to that described above (Section 4.1). However, the contributions of additional, configurationally different electronic states of the system may sometimes be more important than those that implicate the bridging ligand's LUMO. For example, the two lowest energy π* (antibonding) orbitals of pyridine are relatively close in energy (they correlate with the degenerate components of the LUMO of benzene). One of these orbitals has orbital coefficients on all atoms (this is designated the α orbital pattern) and the other has a nodal plane, orthogonal to the ring, which passes through two opposite atoms (designated the β pattern). Both of these orbitals must be considered in many spectroscopic discussions, and they can both contribute to the electron-transfer properties with bridging ligands such as 2,3-*bis*-(2-pyridyl)pyrazine (dpp) [60]. This ligand has been used in the construction of extended arrays of transition metal complexes that might be useful for photonic energy collection, photoinduced oxidation-reduction processes, etc. [120–125]. The π-orbitals of the pyridine and pyrazine moieties of this bidentate ligand differ in energy, and they do not mix as simply as those of the closely related bipyridines. The LUMO and LUMO + 1 of dpp ligand configured to coordinate a single metal are shown in Fig. 15 (HF/LANL2DZ level of computations [126]) [60]. The pyrazine moiety of the dpp LUMO correlates with the pyrazine LUMO + 1, and it has relatively small orbital coefficients on the pyrazine nitrogen atoms. This should correspond to relatively poor LUMO-mediated metal/ligand

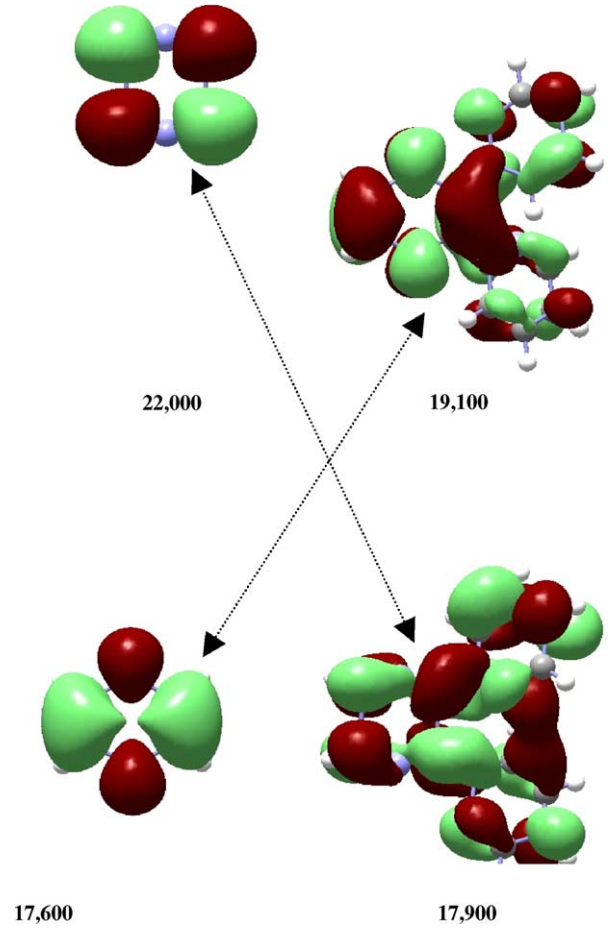

Fig. 15. Computed LUMO (left) and LUMO+1 (right) orbital structures for pyrazine (top) and dpp (bottom). The double-headed arrows indicate the correlated orbital structures of the pyrazine moieties. Computed energies are in cm^{-1}. From [60].

configurational mixing and a correspondingly small value of H_{RP}^{spx} for a D/A pair bridged by this ligand; the configurational mixing mediated by LUMO + 1 should be comparable to that typical of pyrazine-bridged D/A pairs. Since H_{RP}^{spx} is a sum of the contributions from all the relevant CT excited states, and since the Ru^{II}/dpp MLCT transitions that correlate with LUMO and LUMO + 1 are reasonably close in energy [60] this does not have much of an effect on the observed MMCT transition of $[\{Ru(NH_3)_4\}_2dpp]^{5+}$ (it is very similar to that of $[\{Ru(NH_3)_5\}_2pz]^{5+}$ [9] except in band shape [127]). There may be a larger effect for the MLCT excited states: $[Ru(NH_3)_4dpp]^{2+}$ has two MLCT bands of similar energy (18.3×10^3 and $21.9 \times 10^3\ cm^{-1}$) and absorptivity (4500 and 4800 $M^{-1}\ cm^{-1}$, respectively) in ambient aqueous solution, while $[\{Ru(NH_3)_4\}_2dpp]^{5+}$ exhibits a single absorption in this region (at $17.9 \times 10^3\ cm^{-1}$), but with much greater absorptivity (9500 $M^{-1}\ cm^{-1}$/Ru) [60]. This suggests a Jahn-Teller splitting of the higher energy MLCT excited state (correlated with LUMO + 1) that is typical of very strong (D/A) mixed valence coupling.

4.3.2. Summary of observations on selected bridged D/A complexes

The studies cited in this section have dealt with the implications of the electron-transfer absorption and emission spectra of three different classes of linked D/A complexes. These observations, and some evolution of theoretical approaches complement the early studies of Taube and coworkers [13]. For strongly coupled systems in which electron-transfer ground and excited states are both lower in energy than the mediating donor/bridging ligand MLCT excited state (all energies with respect to the ground state coordinates), the results of these studies can be combined in summary form:

a. Configurational mixing with a higher energy charge transfer excited state involving the bridging ligand enhances the electronic coupling of the donor and acceptor when there is good overlap with the donor and acceptor orbitals.
b. The enhanced electronic coupling is manifested in increased absorptivity and lower energy of the D/A MMCT transition.
c. Details of the linker electronic structure are sometimes important in determining the effectiveness of the bridging ligand in facilitating electron-transfer processes.
d. Electronic coupling between the electron-transfer partners (donor and acceptor) and the bridging ligand can alter the properties of the bridging ligand, sometimes even altering the nuclear coordinates within the bridge.
e. Vibronic coupling to the bridging ligand can interfere with super exchange coupling of a bridged donor and acceptor.

5. High frequency vibronic contributions to the electron-transfer emission spectra of cyanide-bridged complexes and electron-transfer behavior in the Marcus-inverted region

Many of the $[\{Ru(NH_3)_5\}_n\{Cr(L)(CN)_n\}]^{(n+3)+}$ complexes (L an am(m)ine ligand; n = 1,2) emit [128,129] at 77 K; see Fig. 16 and Table 3. This is the only class of complexes that has been found to exhibit a transition metal-to-transition metal electron-transfer emission. The maxima of these electron-transfer emissions occur in the 800–850 nm region of the near-infrared, and the 77 K excited state lifetimes are on the order of a microsecond. Am(m)ine perdeuteration of these complexes results in much longer lifetimes, and the size of the isotope effects tend to increase ($k_{NH}/k_{ND} \approx 15$–30) with the number of am(m)ine moieties. The very large isotope

Table 3
Absorption and emission spectral data for cyanide-bridged complexes[a]

Complexes	$Ru_t^{II} \rightarrow M_c^{III}$[b]	$Ru^{II} \rightarrow Ru^{III}$[c]	MMCT emission[d]
	$\lambda_{max}(\varepsilon_{max}/Ru)\ [\Delta\nu_{1/2}]$ (water)	$\lambda_{max}(\varepsilon_{max})[\Delta\nu_{1/2}]$ (water)	$h\nu_{max}[h\nu_{0'0}](\Delta\nu_{1/2})$ (DMSO/water)
trans-$[([14]aneN_4)Cr(CNRu(NH_3)_5)_2]^{5+}$	507(4.0)[4.9]	1000(178)[5.1]	12.0[12.1](0.71)
trans-$[(ms\text{-}Me_6[14]aneN_4)Cr(CNRu(NH_3)_5)_2]^{5+}$	522(4.1)[5.0]	952(160)[4.9]	11.8[11.9](0.76)
trans-$[([15]aneN_4)Cr(CNRu(NH_3)_5)_2]^{5+}$	515(3.6)[4.6]	990(161)[4.9]	11.8[12](0.9)
trans-$[(ms\text{-}Me_6[14]aneN_4)Co(CNRu(NH_3)_5)_2]^{5+}$	513(0.70)[6.0]	890(141)[5.3]	–
trans-$[([14]aneN_4)Rh(CNRu(NH_3)_5)_2]^{5+}$	342(0.40)[6.0][e]	848(75)[6.6]	–
trans-$[(ms\text{-}Me_6[14]aneN_4)Rh(CNRu(NH_3)_5)_2]^{5+}$	330(0.43)[5.9][e]	858(69)[6.1]	–
trans-$[([15]aneN_4)Rh(CNRu(NH_3)_5)_2]^{5+}$	340(0.45)[6.1][e]	865(81)[6.0]	–
trans-$[(py)_4Ru(CNRu(NH_3)_5)_2]^{4+}$	–	1000(1500)[6.2]	–
cis-$[(rac\text{-}Me_6[14]aneN_4)Cr(CNRu(NH_3)_5)_2]^{5+}$	525(4.1)[5.1]	840(150)[5.4]	–
cis-$[([14]aneN_4)Rh(CNRu(NH_3)_5)_2]^{5+}$	340(0.15)[e]	976(145)[4.8]	–
cis-$[(rac\text{-}Me_6[14]aneN_4)Rh(CNRu(NH_3)_5)_2]^{5+}$	345(0.20)[e]	848(67)[5.2]	–
cis-$[([15]aneN_4)Rh(CNRu(NH_3)_5)_2]^{5+}$	343(0.20)[e]	850(137)[5.2]	–

[a] From [128–131].
[b] MM′CT absorption; units: λ_{max}, nm($\varepsilon_{max}/10^3$/Ru, $M^{-1}\ cm^{-1}$)[$\Delta\nu_{1/2}/10$, cm^{-1}.
[c] MMCT absorption; units: λ_{max}, nm(ε_{max}, $M^{-1}\ cm^{-1}$)[$\Delta\nu_{1/2}/10^3$,cm^{-1})].
[d] Units: $h\nu_{max}/10^3$,cm^{-1}[$h\nu_{0'0}/10^3$, cm^{-1}] ($\Delta\nu_{1/2}/10^3$, cm^{-1}), The fundamental emission component, $h\nu_{0'0}$, is based on a Gaussian deconvolution of the emission spectrum; $\Delta\nu_{1/2}$ = the full-width at half height for the fundamental.
[e] Probably mixed with $Ru^{II}/CN^-(\pi^*)$MLCT.

effects suggest a nuclear tunneling mechanism for excited state electron-transfer that is mediated by the N-H stretch. This in turn implies that there should be a vibronic contribution to the electron-transfer emission that arises from the N–H stretch.

5.1. Some details of the emission spectra

The 77 K emission spectrum of $[\{Ru(NH_3)_5\}_2([14]aneN_4)Cr(CN)_2]^{5+}$ (Fig. 16a) is similar in many ways to that of $[Ru(NH_3)_4bpy]^{2+}$ (Fig. 3). The bands are reasonably broad, extending to about 1200 nm consistent with weak vibronic contributions, and they are dominated by an intense fundamental ($\{e, 0'\} \rightarrow \{g, 0\}$) component. The high frequency vibronic contributions are most clearly exhibited in the emrep in Fig. 16b. There are several important features of the electron-transfer emission in these complexes [128–131]: (a) the vibronic contributions are weak and this suggests that the excited state is not greatly distorted; (b) the largest reorganizational energy contributions are in the 500–900 cm^{-1} region; (c) there are C≡N stretching contributions to the electron-transfer reorganizational energy (Fig. 16c); (d) the observed NH/ND isotope effects for the excited state decay rate constants are very large [128,129].

The energy of the emission maximum, the overall emission bandwidth and the emission lifetime are all functions of the excitation energy for these complexes. The variations are systematic and these three properties of the emission all increase systematically as the excitation energy increases [128,129]. When the excitation energy is significantly larger than the (ambient) Ru^{II}/Cr^{III} MM′CT absorption maximum, most of the complexes develop a shoulder on the high-energy side of the emission, and for one complex, *trans*-[(*ms*-Me_6[14]$aneN_4$)Cr (CN $Ru(NH_3)_5)_2]^{5+}$, high-energy excitations result in a new emission band similar to the $(^2E)Cr^{III}$ *dd* emission of the parent dicyano complex [129]. Thus, it appears that the chromium centered *dd*(^{2}E) and the MM′CT excited states have very similar energies in these complexes. The Cr^{II} center of the MM′CT excited state can have either a high spin ($d\pi^3d\sigma$; quintet spin multiplicity) or a low spin ($d\pi^4$; doublet spin multiplicity) electronic configuration, so the net spin multiplicity of the excited state (formally with Cr^{II} and Ru^{III} centers) can be sextet or quartet (for high spin Cr^{II}), or quartet or doublet (for low spin Cr^{II}). A quartet excited state would be expected to relax too rapidly to the quartet ground state to be observed. The excited state with doublet spin multiplicity (low spin Cr^{II}) is most consistent with the small amplitudes of the vibronic contributions to the emission. The ^{2}MM′CT excited state is expected to be stabilized by configurational mixing with the near in energy $(^2E)Cr^{III}$ excited state; these two excited states form a mixed valence pair. Such configurational mixing will distort the MM′CT excited state resulting in a decrease of its energy, a shift of its PE minimum (decreasing the amount of distortion) and reducing the curvature of the PE surface compared to the corresponding diabatic PE surface.

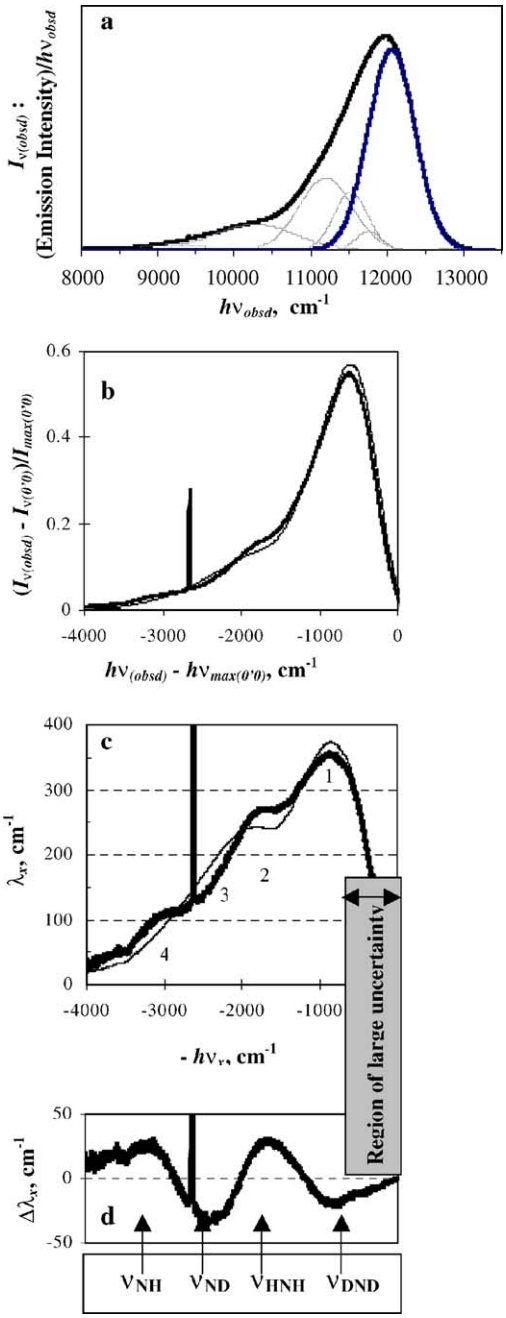

Fig. 16. (a) The MMCT emission spectrum (heavy line) of $[Cr([14]aneN_4)(CNRu(NH_3)_5)_2]^{5+}$ (DMSO/water) at 77 K. Deconvoluted Gaussian fundamental (blue curve) [130]. (b) the difference between the observed spectrum and the fundamental for: (CrCNRu(NH)), heavy line, and (CrCNRu(ND)), light line; (c). the empirical reorganizational energy profiles of (CrCNRu(NH)), heavy line, and of (CrCNRu(ND)), light line; (d) the difference of those profiles. Vibrations of energy $h\nu_x$ in (d) can be associated with the reorganizational energy contributions (in cm^{-1}; tentative assignments in parenthesis) in the ranges: 1, 400–800 (metal–ligand stretch; M-N-H bend); 2, 1500–2000 (C≡N stretch; NH_2 bend); 3, 2100–2700 (N-D stretch); 4, 2900–3600 (N-H stretch). Data from [130,131].

Dominant distortions in the metal–ligand skeletal modes (<1000 cm^{-1}) are consistent with Ru/Cr electron-transfer process that generates the excited state; the breadth of the dominant contribution to Fig. 16b suggests that there are contributions from several skeletal modes. The shoulder at about 2000 cm^{-1} in the emrep of Fig. 16b is consistent with a contribution of the CN-stretching modes to the reorganizational energy. There could be some second order vibronic contributions (j = 2 in Eqs. (2)–(4) and (32)) in this region from vibrations with $\nu_h \approx 1000\,cm^{-1}$ and first order contributions from the HNH bending vibration; even allowing for the largest magnitudes of other contributions, the reorganizational energy contribution of the CN stretching modes is probably greater than about 100 cm^{-1}. The difference in the emreps of $[([14]aneN_4)Cr(CNRu(NH_3)_5)_2]^{5+}$ and $[(d_4\text{-}[14]aneN_4)Cr(CNRu(ND_3)_5)_2]^{5+}$, Fig. 16c, demonstrates the reorganizational energy contributions from N-H stretching modes ($\sim$3200 cm^{-1}) and NH_2 bending modes ($\sim$1600 cm^{-1}), with λ_{NH} and λ_{HNH} both in the range of 25–30 cm^{-1}. The emreps display the contributions of high frequency vibrational modes ($h\nu_h > 4k_BT$) that contribute to the differences in the geometry of the ground and excited electronic states; the amplitudes of the envelope of these contributions (the reorganizational energy profile) at different vibrational frequencies indicate the relative importance of the corresponding distortion modes. These high frequency distortion modes are expected to be very important in determining the electron-transfer rate constant in the Marcus inverted region, and therefore, in determining the electron-transfer excited state lifetime at 77 K.

5.2. Excited state-to-ground state back electron-transfer dynamics of cyanide-bridged complexes

The excited state lifetimes of the Cr(CN)Ru complexes are relatively long compared to closely related classes of complexes. Thus, the $[(NH_3)_5Ru(CNM(CN)_5)]^-$ complexes (M = Fe, Ru, Os) have lifetimes of <1 ps under ambient conditions [132–134], while the electronically excited $[([14]aneN_4)Cr(CNRu(NH_3)_5)_2]^{5+}$ complex has an excited state lifetime of about 7 ns under ambient conditions and about 1 μs at 77 K [128,130]. The back electron-transfer in the $[(NH_3)_5Ru(CNM(CN)_5)]^-$ complexes apparently occurs before the electronic excited state is vibrationally equilibrated, and populates a vibrationally excited state of the ground state [133–135]. The much longer lifetimes of the Cr(CN)Ru complexes is typical of transition metal excited states which differ in spin multiplicity from the ground state. The $[(NH_3)_5Ru(CNM(CN)_5)]^-$ complexes (M = Fe, Ru, Os) necessarily have the same spin multiplicities (doublet) in their lowest energy electron-transfer excited states and in their ground states.

Electronic coupling and high frequency vibrational modes tend to be relatively important in determining excited state lifetimes at low temperatures. It is characteristic of transition metal spectroscopy that the electronic states initially populated by light absorption relax extremely rapidly to the lowest energy excited state (typically within a few ps), and that the lowest energy excited states which are observed to have reasonably long lifetimes (ns to ms) differ in spin multiplicity from the ground state [136]. This is only a variation of the very well known feature of the photophysics of organic molecules that triplet excited states tend to have much longer lifetimes than the configurationally related singlet excited states [137]. However, the rapid relaxation of upper excited states of at least some transition metal complexes appears to involve crossings between states of different electronic configurations that are more rapid than vibrational relaxation within an electronic state [97,138–141], and this is different from the usual experience with organic photophysics [137,142]. These rapid excited state configurational crossings are better described as vibronic transitions, between vibrational levels of the configurationally different states, rather than in terms of Born-Oppenheimer approximation-based PE surfaces illustrated in Figs. 2 and 10. One mechanism for such fast interconfigurational and intersystem crossings is that they involve entangled nuclear and electronic coordinates, and that they are a characteristic of strongly coupled electronic configurations. In contrast, it is generally assumed that the spin multiplicity difference of the ground and excited state, for emitting molecules, contributes to a small matrix element, leading to a weak-coupling limit description for the non-radiative relaxation rate constant.

In glasses at low temperature or in solids, most of the solvent modes are frozen [143]. Eq. (21) is not applicable to the limit in which there is no solvent reorganizational contribution and in which there are no contributing low frequency molecular distortion modes. In this limit, electron-transfer must occur by means of a nuclear tunneling pathway. Nuclear tunneling is most important for the highest frequency distortion modes, and an appropriate expression for this limit and a single contributing high frequency vibrational mode is [35],

$$k_{nr}^0 = H_{PR}^2\left[\frac{8\pi^3}{h^3\nu_h E_{PR}^{0'0}}\right]^{1/2} e^{(-\gamma_h E_{PR}^{0'0}/h\nu_h)} \tag{80}$$

$$\gamma_h \cong \ln\left(\frac{E_{PR}^{0'0}}{\lambda_h}\right) - 1$$

Fig. 16d demonstrates that a small, finite value of λ_{NH} contributes to the emission spectrum of $[\{Ru(NH_3)_5\}_2([14]aneN_4)Cr(CN)_2]^{5+}$. This value in Eq. (80) leads to $k_{nr}^0 \sim 0.5\,H_{PR}^2\,s^{-1}$. It has been estimated for the spin-allowed configurational mixing of the ground state of this complex with the ^{4}MMCT excited state implies that $H_{RP} \cong 3200\,cm^{-1}$ [109]; this would lead to κ_{el} = 1 in Eq. (13), and Eq. (80) would not be applicable. Eq. (80) is only useful if H_{PR} is a relatively small number, less than about 200 cm^{-1}; a value of this magnitude would lead to $k_{nr}^0 \sim 10^4\,s^{-1}$, or an order of magnitude or so smaller than the observed value. Spin-orbit

coupling is appreciable for transition metal complexes [144] and a value of H_{PR} could be of the order of the value cited, since the differences in energy between the configurationally similar excited states (E_{DQ} for excited doublet and quartet states) are not large (values for the Ru^{II}–bpy singlet and triplet MLCT excited states have been estimated to be in the range of 1000–4000 cm^{-1} [60–62]); for H_{SO} the spin-orbit coupling matrix element, $H_{PR} \approx (H_{SO}/E_{DQ})H_{RP}$. While Eq. (80) in combination with the observed reorganizational parameters somewhat underestimates the NH-mediated tunneling pathway, the small value of λ_{NH} implies that the isotope effect, k_{NH}/k_{ND}, will be very large for the NH-mediated tunneling pathway (e.g., from Eq. (70), $k_{NH}/k_{ND} \geq 500$). The larger reorganizational energy inferred for the cyanide stretch (Fig. 16c) suggests that a CN-mediated tunneling pathway is at least 50 times more favorable (based on Eq. (80)) than the ND-mediated pathway.

The lifetime of $[Ru(NH_3)_4(bpy)]^{2+}$ is about 2.5% of that of $[Cr([14]aneN_4)(CNRu(NH_3)_5)_2]^{5+}$ in 77 K DMSO/water glasses [89]; the isotope effect, k_{NH}/k_{ND}, of the former is only about 12% that of the latter. These observations indicate that nuclear tunneling mediated by the N-H stretch is more important for the cyanide-bridged Ru/Cr complex than for the Ru–bpy complex. Small values of λ_{NH} are inferred for both of these complexes; this suggest that if a nuclear tunneling pathway dominates the relaxation behavior, then the NH/ND isotope effect should be very large (probably larger than 10^2). The small isotope effect combined with the short excited state lifetime suggests that some other relaxation channel is more efficient than the NH-mediated nuclear tunneling channel for non-radiative relaxation of the MLCT excited state of $[Ru(NH_3)_4(bpy)]^{2+}$. The very large value of $H_{RP} \approx 7000\ cm^{-1}$ inferred for the ground state/^{1}MLCT excited state mixing in this complex [60] implies that configurational mixing must be very large in the region of the diabatic excited state PE minimum; one effect of this mixing is the attenuation of reorganizational energy illustrated in Fig. 9. This configurational mixing would lead to shifts of the PE minima along the nuclear displacement modes and raises the possibility that the magnitude of the electronic coupling is a function of these shifts (and the nuclear coordinates).

6. Summary

The systematic evaluation of the effects of configurational mixing between electron-transfer ground and excited states on the properties of transition metal donor/acceptor complexes requires the integration of a range of theoretical concepts and experimental techniques, as was clear in the early work of Hush and of Taube. The extensive configurational mixing between electron-transfer states in the strong coupling limit results in distortions of the reactants and products PE surfaces. The magnitude of these distortions can be expressed in terms of the electronic coupling matrix element and vertical energy differences, or in terms of the fraction of delocalized electron density, and the resulting perturbational corrections of the expressions appropriate to the weak-coupling limit. The perturbation theory-based corrections of the weak-coupling limit enable one to systematically evaluate the trends in the properties of related complexes. As in any such comparison, one needs to define a reference state with respect to which the molecular properties of a strongly coupled system are evaluated. A useful and experimentally accessible reference state for complexes in which the electronic coupling is strong can be based on the Franck-Condon parameters obtained from ion pair absorption spectra, outer-sphere electron-transfer kinetics and/or the electrochemical properties of structurally equivalent mono-metallic complexes. It is a characteristic of transition metal complexes that there are sometimes many electronic states in a relatively small energy range. This can result in excited state properties that do not conform to simple models. Configurational mixing can then result in unexpected properties of the electron-transfer system.

This article has focused on three classes of strongly coupled, covalently linked transition metal donor/acceptor complexes: (a) the directly linked D/A, ruthenium bipyridine complexes; (b) complexes with cyanide or cyano-complex bridges; (c) complexes with polypyridine bridges linking the donor and acceptor. These complexes illustrate important features of the limit in which D/A electronic coupling is very strong:

a. Reorganizational energies are very strongly attenuated with increases in the ground state-excited state configurational mixing (e.g., as $(1 - 4\alpha_{RP}^2)$ for absorption and $(1 - 2\,\alpha_{RP}^2 - 2\,\alpha_{PR}^2)$ for emission). The evaluation of the reorganizational energy contributions of high frequency vibrational modes to the 77 K emission spectra and the relatively small k_{NH}/k_{ND} isotope effects of am(m)ine-bipyridine–ruthenium complexes indicates that nuclear tunneling mediated by NH stretching modes is overwhelmed by some more efficient excited state relaxation channel. This unique channel may be correlated with the large electronic matrix element and the very appreciable configurational mixing in these complexes.
b. Many of the polypyridine bridged complexes studied by the Taube group illustrate the systematic decrease of the energy of the MM′CT absorption as the superexchange contribution to electronic coupling increases.
c. The cyanide-bridged, donor–acceptor complexes have allowed us to explore many previously little known aspects of electron-transfer chemistry: (i) they have provided nice examples of the consequences of the limit in which D/A electronic coupling depends on the nuclear coordinates within the bridging ligand; (ii) they have provided the first examples of electron-transfer emission in transition metal D/A complexes; (iii) they have provided examples of systems in which bridging ligand vibrational modes contribute to the electron-transfer reorganizational energy.

7. Problems and extensions

Some issues noted above, or related to the material discussed here are not fully resolved and/or under current investigation. Among these issues are:

a. The attenuation of reorganizational energies for spin forbidden transitions (as in phosphorescent emission spectra) is expected to be approximately $(1 - 2\alpha_{RP}^2 - 2\alpha_{PR}^2)$, where $\alpha_{RP} > \alpha_{PR}$ (see Section 5.1.a(iv) above), but there is not yet much experimental evidence [89].
b. Almost all superexchange arguments assume that the vertical energy for the electronic transition from the ground state to the electron-transfer excited state is smaller than that for transition to the bridging ligand MLCT excited state that mediates the electronic coupling. If the transition energies are in the reversed order, then the MMCT transition energies should increase rather than decrease, with the extent of configurational mixing. Other features of this limit are not yet clear.
c. When D/A electronic coupling is sufficiently strong, the electron-transfer hopping frequency and the frequency of some vibrational motions in the molecule may couple. The work of Ito, Kubiak and co-workers on pyrazine-bridged, mixed valence ruthenium clusters may provide an example of this behavior [145–149], and Meyer and co-workers have raised this issue in regard to $[\{Ru(NH_3)_5\}_2pz]^{2+}$ and some related complexes [20].

Acknowledgement

The authors thank the Office of Basic Energy Sciences of the Department of Energy for partial support of this research.

References

[1] H. Taube, Can. J. Chem. 37 (1959) 129.
[2] T.J. Meyer, H. Taube, in: G. Wilkinson (Ed.), Comprehensive Coordination Chemistry, Pergamon Press, Oxford, 1987.
[3] D.E. Richardson, H. Taube, Coord. Chem. Rev. 60 (1984) 107.
[4] V. Balzani (Ed.), Electron Transfer in Chemistry, Wiley-VCH, Weinheim, 2001.
[5] N.S. Hush, Electrochim. Acta 13 (1968) 1005.
[6] N.S. Hush, Prog. Inorg. Chem. 8 (1968) 391.
[7] N.S. Hush, in: D.B., Rorabacher, J.F., Endicott (Eds.), Mechanistic Aspects of Inorganic Reactions, ACS Symposium Series 198, American Chemical Society, Washington, 1982.
[8] C. Creutz, H. Taube, J. Am. Chem. Soc. 91 (1969) 3988.
[9] C. Creutz, H. Taube, J. Am. Chem. Soc. 95 (1973) 1086.
[10] J.E. Sutton, P.M. Sutton, H. Taube, Inorg. Chem. 18 (1979) 1017.
[11] J.E. Sutton, H. Taube, Inorg. Chem. 20 (1981) 4021.
[12] D.E. Richardson, J.P. Sen, H. Taube, Inorg. Chem. 21 (1982) 3136.
[13] D.E. Richardson, H. Taube, J. Am. Chem. Soc. 105 (1983) 40.
[14] P.A. Lay, R.H. Magnuson, H. Taube, J. Am. Chem. Soc. 105 (1983) 2507.
[15] P.A. Lay, R.H. Magnuson, H. Taube, Inorg. Chem. 27 (1988) 2364.
[16] C. Creutz, Progr. Inorg. Chem. 30 (1983) 1.
[17] B.S. Brunschwig, C. Creutz, N. Sutin, Chem. Soc. Rev. 31 (2002) 168.
[18] C. Creutz, M.D. Newton, N. Sutin, Photochem. Photobiol. A: Chem. 82 (1994) 47.
[19] R. Crutchley, Adv. Inorg. Chem. 41 (1994) 273.
[20] K.D. Demadis, C.M. Hartshorn, T.J. Meyer, Chem. Rev. 101 (2001) 2655.
[21] J.F. Endicott, in: J. McCleverty, T.J. Meyer (Eds.), Comprehensive Coordination Chemistry II, vol. 7, Pergamon Press, Oxford, 2003.
[22] M.D. Newton, Chem. Rev. 91 (1991) 767.
[23] M.D. Newton, in: V. Balzani (Ed.), Electron Transfer In Chemistry, Wiley-VCH, Weinheim, 2001.
[24] D.E. Richardson, in: E.I. Solomon, A.B.P. Lever (Eds.), Inorganic Electronic Structiure and Spectroscopy, Wiley, New York, 1999.
[25] W. Kaim, A. Klein, M. Glockle, Acc. Chem. Res. 33 (2000) 755.
[26] A.B.P. Lever, E. Dodsworth, in: A.B.P. Lever, E.I. Solomon (Eds.), Electronic Structure and Spectroscopy of Inorganic Compounds, vol. II, Wiley, New York, 1999.
[27] S.I. Gorelsky, V.Y. Kotov, A.B.P. Lever, Inorg. Chem. 37 (1998) 4584.
[28] P.F. Barbara, T.J. Meyer, M. Ratner, J. Phys. Chem. 100 (1996) 13148.
[29] R.A. Marcus, Discuss. Faraday Soc. 29 (1960) 21.
[30] R.A. Marcus, Annu. Rev. Phys. Chem. 15 (1964) 155.
[31] R.A. Marcus, J. Chem. Phys. 43 (1965) 670.
[32] R.A. Marcus, N. Sutin, Comments Inorg. Chem. 5 (1986) 119.
[33] R.A. Marcus, N. Sutin, Biochem. Biophys. Acta 811 (1985) 265.
[34] D.N. Beratan, J.N. Betts, J.N. Onuchic, Science 252 (1991) 1285.
[35] R. Englman, J. Jortner, Mol. Phys. 18 (1970) 145.
[36] K.F. Freed, J. Jortner, J. Chem. Phys. 52 (1970) 6272.
[37] J. Jortner, M. Bixon (Eds.), Adv. Chem. Phys., 1999.
[38] N. Kestner, J. Logan, J. Jortner, J. Phys. Chem. 64 (1974) 2148.
[39] A.A. Kornyshev, M. Tosi, J. Ulstrup (Eds.), Electron and Ion Transfer in Condensed Media, World Scientific, Singapore, 1997.
[40] A.M. Kuznetsov, Charge Transfer in Physics, Chemistry and Biology: Physical Mechanisms of Elementary Processes and An Introduction to the Theory, Gordon and Breach, New York, 1995.
[41] D.V. Matyushov, G.A. Voth, in: K.B. Lipkowitz, D.B. Boyd (Eds.), Reviews in Computational Chemistry, Wiley-VCH, New York, 2002.
[42] M.D. Newton, Adv. Chem. Phys. 106 (1999) 303.
[43] M.D. Newton, N. Sutin, Annu. Rev. Phys. Chem. 35 (1984) 437.
[44] S.B. Piepho, E.R. Krausz, P.N. Schatz, J. Am. Chem. Soc. 100 (1978) 2996.
[45] M.A. Ratner, Nature 397 (1999) 480.
[46] M. Bixon, J. Jortner, J. Cortes, H. Heilte, M.E. Michel-Beyerle, J. Phys. Chem. 98 (1994) 7289.
[47] M. Bixon, B. Giese, S. Wessely, T. Langenbacher, M.E. Michel-Beyerle, J. Jortner, Proc. Natl. Acad. Sci. U.S.A. 96 (1999) 11713.
[48] H. Sumi, in: V. Balzani (Ed.), Electron Transfer in Chemistry, vol. 1, Wiley-VCH, Weinheim, 2001.
[49] A. Warshel, Acc. Chem. Res. 35 (2002) 385.
[50] R.D. Cannon, Electron Transfer Reactions, Butterworth, London, 1980.
[51] N. Sutin, Acc. Chem. Res. 15 (1982) 275.
[52] B.S. Brunschwig, N. Sutin, in: V. Balzani (Ed.), Electron Transfer in Chemistry, Wiley-VCH, Weinheim, 2001.
[53] I.R. Gould, D. Noukakis, G.-J. Luis, R.H. Young, J.L. Goodman, S. Farid, Chem. Phys. 176 (1993) 439.
[54] A.B. Myers, Acc. Chem. Res. 30 (1998) 519.
[55] A.B. Myers, in: A.B. Myers, T.R. Rizzo (Eds.), Laser Techniques in Chemistry, Wiley, 1995.
[56] T.C. Brunold, H.U. Gudel, in: E.I. Solomon, A.B.P. Lever (Eds.), Inorganic Electronic Structure and Spectroscopy, Wiley, New York, 1999.

[57] E. Krausz, H. Riesen, in: E.I. Solomon, A.B.P. Lever (Eds.), Inorganic Electronic Structure and Spectroscopy, Wiley, New York, 1999.
[58] A.B. Myers, Chem. Rev. 96 (1996) 911.
[59] R.A. Marcus, J. Phys. Chem. 93 (1989) 3078.
[60] D.S. Seneviratne, M.J. Uddin, V. Swayambunathan, H.B. Schlegel, J.F. Endicott, Inorg. Chem. 41 (2002) 1502.
[61] A.B.P. Lever, S.I. Gorelsky, Coord. Chem. Rev. 208 (2000) 153.
[62] J.F. Endicott, H.B. Schegel, M.J. Uddin, D. Senerivatne, Coord. Chem. Rev. 229 (2002) 95.
[63] J.F. Endicott, M.J. Uddin, H.B. Schlegel, Res. Chem. Intermed. 28 (2002) 761.
[64] E.I. Solomon, Comments Inorg. Chem. 3 (1984) 227.
[65] J.T. Hupp, R.T. Williams, Acc. Chem. Res. 34 (2001) 808.
[66] K. Maruszewski, K. Bajdor, D.P. Strommen, J.R. Kincaid, J. Phys. Chem. 99 (1995) 6286.
[67] H. Yersin, D. Braun, G. Hensler, E. Galhuber, in: C.D. Flint (Ed.), Vibronic Processes in Inorganic Chemistry, Kluwer, Dordrecht, 1989.
[68] N. Sutin, Prog. Inorg. Chem. 30 (1983) 441.
[69] J.F. Endicott, in: V. Balzani (Ed.), Electron Transfer in Chemistry, vol. 1, Wiley-VCH, New York, 2001.
[70] J.F. Endicott, M.J. Uddin, Coord. Chem. Rev. 219–221 (2001) 687.
[71] J.T. Yardley, Introduction to Molecular Energy Transfer, Academic, New York, 1980.
[72] R.S. Mulliken, W.B. Person, Molecular Complexes, Wiley, New York, 1967.
[73] B.S. Brunschwig, C. Creutz, N. Sutin, Coord. Chem. Rev. 177 (1998) 61.
[74] R.J. Campion, C.F. Deck, P. King Jr., A.C. Wahl, Inorg. Chem. 6 (1967) 672.
[75] D.H. Macartney, Inorg. Chem. 30 (1991) 3337.
[76] A. Zahl, R. van Eldik, T.W. Swaddle, Inorg. Chem. 41 (2002) 757.
[77] R. Billing, D.E. Khoshtariya, Inorg. Chem. 33 (1994) 4038.
[78] X. Song, Y. Lei, S. Van Wallendel, M.W. Perkovic, D.C. Jackman, J.F. Endicott, D.P. Rillema, J. Phys. Chem. 97 (1993) 3225.
[79] C.M. Elliott, D.L. Derr, D.V. Matyushov, M.D. Newton, J. Am. Chem. Soc. 120 (1998) 11714.
[80] R. Berkhoff, K. Krist, H.D. Gafney, Inorg. Chem. 19 (1980) 1.
[81] D. Graff, J.P. Claude, T.J. Meyer, in: S.S. Isied (Ed.), Electron Transfer in Organometallic and Biochemistry, American Chemical Society, Washington, 1997.
[82] P. Chen, T.J. Meyer, Chem. Rev. 98 (1998) 1439.
[83] J.R. Reimers, N.S. Hush, J. Phys. Chem. 95 (1991) 9773.
[84] A. Ferretti, A. Lami, G. Villani, Inorg. Chem. 37 (1998) 2799.
[85] D.V. Matyushov, M.D. Newton, J. Phys. Chem. A 105 (2001) 8516.
[86] D.V. Matyushov, G.A. Voth, J. Phys. Chem. A 104 (2000) 6470.
[87] Y.K. Shin, B.S. Brunschwig, C. Creutz, N. Sutin, J. Phys. Chem. 100 (1996) 8157.
[88] P. Xie, Y.-J. Chen, J.F. Endicott, M.J. Uddin, D. Senerivatne, P.G. McNamara, Inorg. Chem. 42 (2003) 5040.
[89] P. Xie, Y.-J. Chen, M.J. Uddin, J.F. Endicott, in preparation.
[90] A. Juris, F. Barigelletti, S. Compangna, V. Balzani, P. Belser, A. von Zelwesky, Coord. Chem. Rev. 84 (1988) 85.
[91] T.J. Meyer, Progr. Inorg. Chem. 30 (1983) 389.
[92] K. Kalyanasundaram, Photochemistry of Polypyridine and Porphyrin Complexes, Academic Press, New York, 1992.
[93] X. Song, J.F. Endicott, Chem. Phys. Lett. 204 (1993) 400.
[94] C.D. Borsarelli, S.E. Brasalvsky, J. Phys. Chem. 102 (1998) 6231.
[95] A.B.P. Lever, Inorganic Electronic Spectroscopy, Elsevier, Amsterdam, 1984.
[96] F.A. Cotton, Chemical Applications of Group Theory, 3rd ed., Wiley, New York, 1990.
[97] J.K. McCusker, Acc. Chem. Res. 36 (2003) 876.
[98] H.M. McConnell, J. Chem. Phys. 35 (1961) 508.
[99] M.D. Newton, J. Electroanal. Chem. 438 (1997) 3.
[100] D.L. Dexter, Phys. Rev. 126 (1962) 1962.
[101] A.V. Macatangay, X. Song, J.F. Endicott, J. Phys. Chem. 102 (1998) 7537.
[102] A.V. Macatangay, J.F. Endicott, Inorg. Chem. 39 (2000) 437.
[103] D.K. Lavalle, E.B. Fleischer, J. Am. Chem. Soc. 94 (1972) 2599.
[104] K. Rieder, H. Taube, J. Am. Chem. Soc. 99 (1977) 7891.
[105] D.H. Oh, S.G. Boxer, J. Am. Chem. Soc. 112 (1990) 8161.
[106] D.H. Oh, M. Sano, S.G. Boxer, J. Am. Chem. Soc. 113 (1991) 6880.
[107] M.A. Watzky, J.F. Endicott, X. Song, Y. Lei, A.V. Macatangay, Inorg. Chem. 35 (1996) 3463.
[108] A.V. Macatangay, S.E. Mazzetto, J.F. Endicott, Inorg. Chem. 38 (1999) 5091.
[109] M.A. Watzky, A.V. Macatangay, R.A. Van Camp, S.E. Mazzetto, X. Song, J.F. Endicott, T. Buranda, J. Phys. Chem. 101 (1997) 8441.
[110] K. Nakamoto, Infrared and Raman Spectra of Inorganic and Coordination Compounds. Part B, Wiley, New York, 1997.
[111] C.J. Ballhausen, in: C.D. Flint (Ed.), Vibronic Processes in Inorganic Chemistry, Kluwer, Dordrecht, 1989.
[112] I.B. Bersuker, The Jahn-Teller Effect and Vibronic Interactions in Modern Chemistry, Plenum, New York, 1984.
[113] J.F. Endicott, M.A. Watzky, A.V. Macatangay, S.E. Mazzetto, X. Song, T. Buranda, in: A.A. Kornyshev, M. Tosi, J. Ulstrup (Eds.), Electron and Ion Transfer in Condensed Media, World Scientific, Singapore, 1997.
[114] J.F. Endicott, M.A. Watzky, X. Song, T. Buranda, Coord. Chem. Rev. 159 (1997) 295.
[115] J.W. Seyler, W. Weng, Y. Zhou, J.A. Gladysz, Organometallics 12 (1993) 3802.
[116] M. Brady, W.Q. Weng, Y.L. Zhou, J.W. Seyler, A.J. Amoroso, A.M. Arif, M. Bohme, G. Frenking, J.A. Gladysz, J. Am. Chem. Soc. 119 (1997) 775.
[117] I.B. Bersuker, S.A. Borshch, Adv. Chem. Phys. 81 (1992) 703.
[118] B.S. Tsukerblat, Group Theory in Chemistry and Spectroscopy, Academic Press, London, 1994.
[119] B. Coe, T.J. Meyer, P.S. White, Inorg. Chem. 34 (1995) 593.
[120] V. Balzani, F. Scandola (Eds.), Supramolecular Photochemistry, Horwood, Chichester, 1991.
[121] V. Balzani, S. Campagna, G. Denti, A. Juris, S. Serroni, D. Venturi, Acc. Chem. Res. 31 (1998) 26.
[122] M. Carano, P. Ceroni, F.C.M. Marcaccio, C. Paradisi, S. Roffia, Electrochim. Acta 46 (2001) 46.
[123] S. Serroni, S. Campagna, F. Puntoriero, A. Juris, G. Denti, V. Balzani, D. Venturi, D. Janzen, K.R. Mann, Inorg. Synth. 33 (2002) 10.
[124] S. Serroni, S. Campagna, F. Puntoriero, F. Loiseau, V. Ricevuto, R. Passalacqua, M. Galletta, Comtes Rendus Chimie 6 (2003) 883.
[125] A.A. Holder, S. Swavey, K.J. Brewer, Inorg. Chem. 43 (2004) 303.
[126] M.J.T. Frisch, G.W. Schlegel, H.B. Scuseria, G.E. Robb, M.A. Cheeseman, J.R. Zakrzewski, V.G. Montgomery, J.A. Stratmann, R.E. Burant, J.C. Dapprich, S. Millam, J.M. Daniels, A.D. Kudin, K.N. Strain, M.C. Farkas, O. Tomasi, J. Barone, V. Cossi, M. Cammi, R. Mennucci, B. Pomelli, C. Adamo, C. Clifford, S. Ochterski, J. Petersson, G.A. Ayala, P.Y. Cui, Q. Morokuma, K. Malick, D.K. Rabuck, A.D. Raghavachari, K. Foresman, J.B. Cioslowki, J. Ortiz, J.V. Stefanov, B.B. Liu, G. Liashenko, A. Piskorz, P. Komaromi, I. Gomperts, R. Martin, R.L. Fox, D.J. Keith, T. Al-Laham, M.A. Peng, C.Y. Nanayakkara, A. Gonzalez, C. Challacombe, M. Gill, P.M.W. Johnson, B.G. Chen, W. Wong, M.W.L Andres, J. Head-Gordon, M. Replogle, E.S. Pople, J.A. Gaussian, Inc., Pittsburgh, PA, 1998.
[127] V. Swayambunathan, J.F. Endicott, Abstracts 208th National Meeting of the A. C. S., Amer. Chem. Soc., Washington, DC 1994; abstract no. INOR 229, 1994.
[128] J.F. Endicott, P.G. McNamara, T. Buranda, A.V. Macatangay, Coord. Chem. Rev. 208 (2000) 61.
[129] P.G. McNamara, Ph.D. Dissertation, Wayne state University, 2001.

[130] Y.-J. Chen, P. Xie, J.F. Endicott, J. Phys. Chem. A 108 (2004) 5041.
[131] Y.-J. Chen, P. Xie, P.G. McNamara, J.F. Endicott, in preparation.
[132] D.A.V. Tominaga, A.E. Kliner, A.E. Johnson, N.E. Levinger, P.F. Barbara, J. Chem. Phys. 98 (1993) 1228.
[133] P.J. Reid, C. Silva, P.F. Barbara, L. Karki, J.T. Hupp, J. Phys. Chem. 99 (1995).
[134] D.H. Son, P. Kambhampati, T.W. Kee, P.F. Barbara, J. Phys. Chem. A 106 (2002) 4591.
[135] S.K. Doorn, R.B. Dyer, P.O. Stoutland, W.W. Woodruff, J. Am. Chem. Soc. 115 (1993) 6398.
[136] J.F. Endicott, in: E.I. Solomon, A.B.P. Lever (Eds.), Electronic Structure and Spectroscopy of Inorganic Compounds, vol. 2, Wiley, New York, 1999.
[137] J.B. Birks, Photophysics of Aromatic Molecules, Wiley, New York, 1970.
[138] N.H. Damarauer, G. Cerullo, A. Yeh, T.R. Boussie, C.V. Shank, J.K. McCusker, Science 275 (1997) 54.
[139] N.H. Damarauer, J.K. McCusker, J. Phys. Chem. A 103 (1999) 8440.
[140] J.E. Monat, J.K. McCusker, J. Am. Chem. Soc. 122 (2000) 4092.
[141] A.T. Yeh, C.V. Shank, J.K. McCusker, Science 289 (2000) 935.
[142] N. Turro, Modern Molecular Photochemistry, Benjamin/Cummings, Menlo Park, CA, 1978.
[143] R.A. Marcus, J. Phys. Chem. 94 (1990) 4963.
[144] B.N. Figgis, M.A. Hitchman, Ligand Field Theory and its Applications, Wiley-VCH, New York, 2000.
[145] T. Ito, T. Hamaguchi, H. Nagino, T. Yamaguchi, H. Kido, I.S. Zavarine, T. Richmond, J. Washington, C.P. Kubiak, J. Am. Chem. Soc. 121 (1999) 4625.
[146] I.S. Zavarine, C.P. Kubiak, T. Yamaguchi, K. Ota, T. Matsui, T. Ito, Inorg. Chem. 39 (2000) 2696.
[147] T. Ito, T. Yamaguchi, C.P. Kubiak, Macromol. Symp. 156 (2000) 269.
[148] C.H. Londergan, J.C. Salsman, S. Ronco, L.M. Dolkas, C.P. Kubiak, J. Am. Chem. Soc. 124 (2002) 6236.
[149] C.H. Londergan, J.C. Salsman, S. Ronco, C.P. Kubiak, Inorg. Chem. 42 (2003) 926.